Theses and Dissertations

2017

A Study of the Prediction of Ammonium Bisulfate Formation Temperature by Artificial Intelligence

Fengxiang Nie
Lehigh University

A STUDY OF THE PREDICTION OF AMMONIUM BISULFATE FORMATION TEMPERATURE BY ARTIFICIAL INTELLIGENCE

by

Fengxiang Nie

Presented to the Graduate and Research Committee

of Lehigh University

in Candidacy for the Degree of

Master of Science

in

Mechanical Engineering

Lehigh University

(August 2017)

This thesis is accepted and approved in partial fulfillment of the requirements for the Master of Science.

_____
Date

_____
Dr. Alparslan Oztekin, Thesis Advisor

_____
Dr. Gary Harlow, Chairperson of Department

ACKNOWLEDGMENTS

I would like to express my greatest appreciation to my thesis advisors, Dr. Alparslan Oztekin and Dr. Carlos E. Romero. Thank you for your guidance and support during my thesis work. I would like to thank Zheng Yao, CJ Pan and Shaojun Ren at the Energy Research Center, for helping me to solve technical question. I also would like to thank my family for their encouragement and support. Thanks Dr. Carlos E. Romero again for that help beyond words.

TABLE OF CONTENTS

LIST OF TABLES

LIST OF FIGURES

ABSTRACT

Ammonium bisulfate (ABS) is an acidic deposit that can form on the metal elements of air preheaters in power boilers, leading to unit operational issues. As a byproduct of the Selective Catalytic Reduction (SCR) systems for nitrogen oxide (NO_x) emissions control, ABS could result in unit efficiency deterioration, even unit outage. ABS formation temperature is an important factor in controlling the issues associated with ABS fouling problems. If the ABS formation temperature could be monitored, the ABS deposition location could be identified. Subsequently, preventative actions could be taken to avoid ABS fouling to develop into a serious operational problem, such as air preheater plugging. This study deals with indirect predictive models of ABS formation temperature. Five models were developed based on data mining technologies, using actual power plant data. Data composed of 14,230 samples, from 49 variables were used in the study. In the modeling, Principal Component Analysis (PCA) and Sensitivity Analysis (SA) were used to reduce the number of variables in the data set. K-Means Clustering (KMC) was also employed to compress training samples. Neural Networks (NN) and Support Vector Machine (SVM) were used for data modeling. Model results were validated with ABS formation temperatures measured with an ABS dew-point probe. A SA was performed to determine the impact of individual variables on the ABS formation process. It was found that four unit variables: SO_2 stack concentration, SCR gas outlet temperature, SCR inlet NO_x concentration and dilution skid ammonia flow, can provide a good representation of

the data set for ABS formation temperature prediction. The most accurate predictive model consists of a sequence of KMC and SVM. This approach can predict ABS formation temperature within a 9% error from the physical measurement.

1 INTRODUCTION

Coal-fired power generation is the most important source of global electricity production, capturing 41% of the electricity market in 2013 [1]. However, despite coal-fired power generation being an efficient and reliable electricity producing technology, it faces strict environmental regulation. Carbon dioxide (CO_2), sulfur oxides (SO_x), NO_x, and particulate matter (PM) are the main pollutants from coal-fired power plants. There is a variety of emissions control technologies for NO_x abatement. SCR is one of these technologies. However, there are issues associated to the installation of SCR systems. ABS fouling of boiler back-end equipment is one of these issues. ABS fouling leads to pressure drop and thermal efficiency impact, resulting in loss of unit availability and power generation. It has been reported that SCR systems in Germany, Japan, and the United States suffer from ABS fouling issues [2].

In this study, a review of ABS formation and its impact on related power plant equipment is first introduced. Given that measurement of ABS formation temperature is a key point to help mitigation of the ABS fouling issue, this study deals with indirect predictive models of ABS formation temperature. Models were developed based on data mining technologies and Artificial Intelligence (AI) tools. Finally, this study reports results of five models, which were developed using actual power plant data. These models were validated with ABS formation temperatures measured with an ABS dew-point probe. It was found that

the combination of data mining and AI can produce ABS predicted temperatures within 10% of the measured temperatures.

1.1 Selective Catalytic Reduction

1.1.1 Background

NO_x is a primary pollutant produced during the combustion process. Nitric oxide (NO) and nitrogen dioxide (NO_2) are the two main components in NO_x. In high temperature combustion, NO_x can be generated by the reaction of oxygen and nitrogen from both air and fuel. It is well documented that NO_x is a precursor of acid rain which is detrimental to human health, buildings and crops. Furthermore, NO_x contributes to ozone formation at the tropospheric level. For this reason, NO_x emissions from combustion sources are regulated, monitored, and require a strict level of control [3].

Pre-combustion fuel switching, combustion control and post-combustion reduction have been applied to reduce NO_x emissions from coal-fired power plants. SCR technology is currently the most effective way of post-combustion NO_x reduction. SCR can reduce more than 90% of NO_x present in coal-fired power plants flue gas [3]. The first SCR was developed in Japan in 1963. SCR is currently used in a variety of power plants such as those fired by coal, natural gas, fuel oil, biomass and refuse.

1.1.2 SCR Process

The SCR process is a mean of converting NO_x, with the aid of a catalyst, into diatomic nitrogen (N_2), and water (H_2O) [4]. Ammonia (NH_3) and urea (CON_2H_4) are normally used as reagents in the SCR process to react with NO_x. As shown in Figure 1, a reagent such as NH_3, is sprayed before the flue gas flows past a catalyst. The catalyst is placed in a big reactor. The main reactions in the reactor are [5]:

$$4NO + 4NH_3 + O_2 \rightarrow 4N_2 + 6H_2O$$

$$NO + NO_2 + 2NH_3 \rightarrow 2N_2 + 3H_2O$$
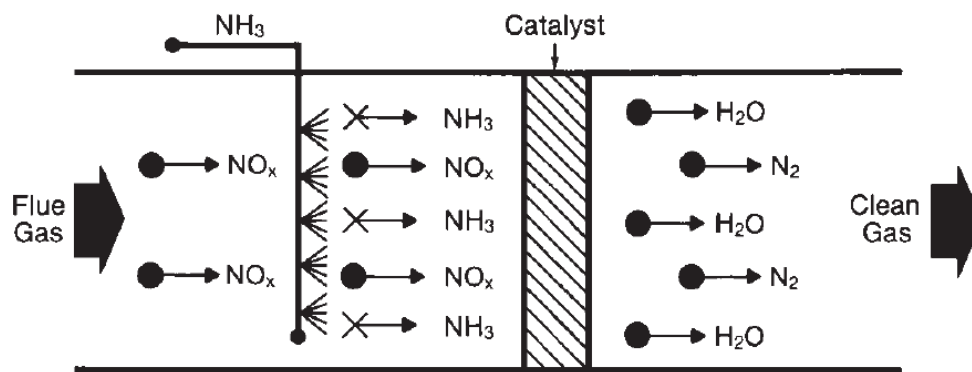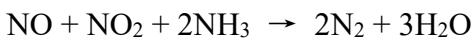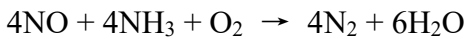
Figure 1. SCR NO_x Removal Process [3]

SCR equipment is usually installed downstream of the economizer in the boiler, as shown in Figure 2. Figure 3 amplifies the SCR portion of Figure 2. Besides the SCR reactor, there is a bypass around the SCR. When the SCR reactor needs to be fallen out of service, operators can modify the damper position so that the flue gas can pass through the SCR bypass and continue the operation of the unit.
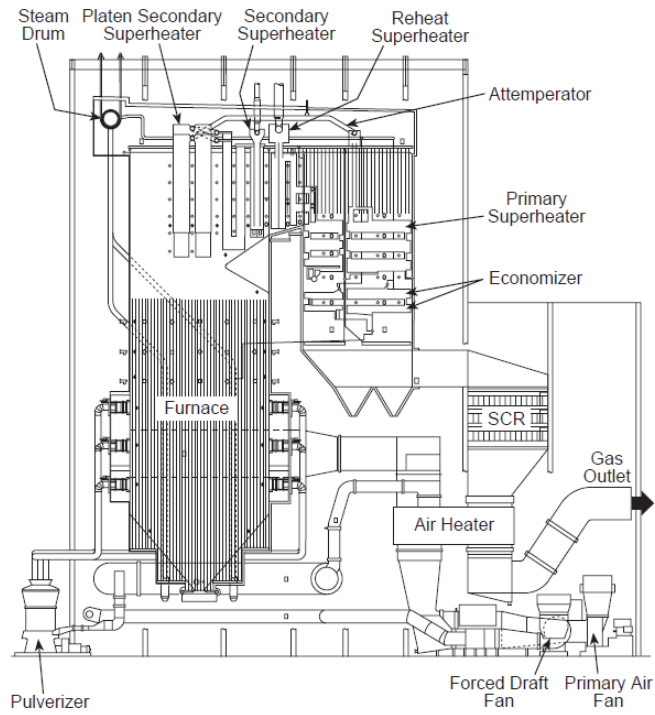
Figure 2. Location of the Air Preheater and SCR in a Coal-Fired Power Plant [3]
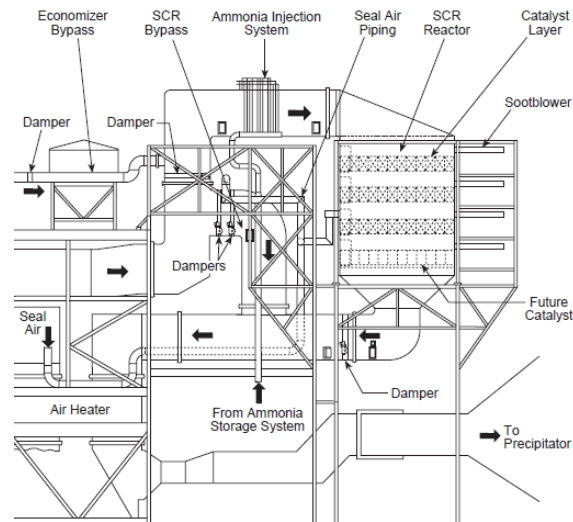
Figure 3. SCR Bypass Damper [3]

1.1.3 Ammonia Slip

NO_x removal efficiency, ammonia utilization, and ammonia slip are three of the most

important indicators of SCR performance. NO_x removal efficiency is defined as, Eff_{NO_x} = $(NO_{x,in} - NO_{x,out})/NO_{x,in}$. Ammonia utilization is similarly defined as, U = (ammonia$_{in}$ - ammonia$_{out}$)/ ammonia$_{in}$. Ammonia slip is highly related to ABS formation. During the NO_x removal process in the SCR, ammonia is injected into the flue gas and most of it reacts with NO_x, converting it to nitrogen. However, some portion of the ammonia passes through the SCR system unreacted. This is so called "ammonia slip" [6]. Reduction of ammonia slip is very important in the operation of SCR systems. Typically, NH_3 is monitored in real time after the SCR reactor. Periodic tuning of the SCR system is also performed couple of times a year to minimize NH_3 carryover.

1.2 Air Preheater

1.2.1 Background

Air preheaters are used in coal-fired power plants to preheat the combustion air and improve the efficiency of the combustion process and the overall efficiency of the boiler. The air preheater transfers heat from the flue gas to the combustion air. This feature increases boiler efficiency 5 to 10%. Additionally, the hot combustion air is also used for drying and transporting the fuel in solid fuel plants. Figure 2 shows a diagram of the air preheater located downstream of the economizer and SCR reactor.

Air preheaters can be classified into recuperative and regenerative types, depending on different operating principle and structure. In the recuperative air preheater, heat is

transferred directly and continuously through stationary and solid heat exchanging surfaces. The regenerative air preheater is more popular than the recuperative air preheater in coal-fired power plants.

1.2.2 Regenerative Air Preheaters

The regenerative air preheater transfers heat indirectly through a storage medium. The storage medium is made up of multiple heating surface elements. Typically, metallic plates like tight packed bundles of corrugated steel are used as the heating surface elements [7]. Heating surface elements are periodically exposed to the hot and cold flow streams as the air preheater turns. There are two types of regenerative air preheaters the Ljungström-type and the Rothemühle-type. The Ljungström air preheater has a fixed cylindrical shell plus a rotor packed with the heating surface elements. The Rothemühle air preheater, rather than fitted with stationary heating surface elements, it has rotating ducts [3]. In coal-fired power plants, the Ljungström type of air preheater is used the most.

Figure 4 shows a representation of a Ljungström air preheater. In this figure, it can be seen the counterflow of air and flue gas through the air preheater, from bottom and top, respectively. The air flows through one half of it while the flue gas flows through the other half. Ljungström air preheaters can be divided into two, three or four sectors, because of the various rotating plate designs. For instance, the tri-sector type divides the air channel into two parts, primary air and secondary air separately (see Figure 5). Therefore, two

sectors of air channel adding one sector of gas channel are three sectors. With respect to the heating surface elements, in the axial direction, this type of air preheater can be divided into two to four layers: hot layer, intermediate layer(s), cold layer, depending on the different metal temperatures.
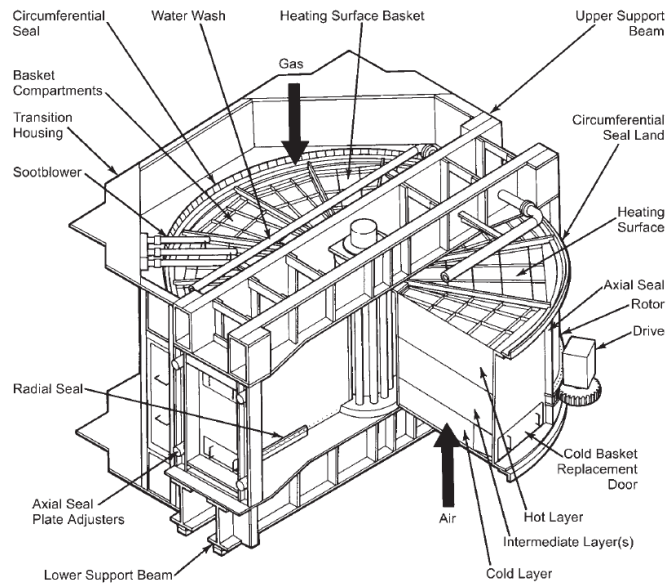
Figure 4. Ljungström-Type Air Preheater [3]
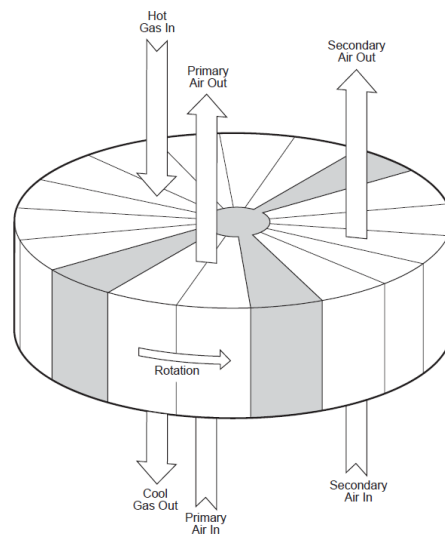
Figure 5. Ljungström-Type Tri-Sector Air Preheater [3]

9

The rotation speed of regenerative air preheaters is quite slow, around 1-3 rpm [3][8], to allow heat to be transferred efficiently. Typical data for Ljungström air preheaters are shown in Table 1.

Table 1. Typical Data for Ljungström-Type Air Preheater [8]

Typical Data for today's sizes of Ljungström Air Preheater

The sizes of boilers have since then increased and below typical data for a modern installation is:

Boiler Size (electrical output)	300 MW	500 MW
Fuel	Coal	Oil
Ljungström Air Preheater Size	2 x 28.5	2 x 30
Diameter (m)	9.9	11.4
Area (m²)	73	97
Height(m)	2.0	1.8
Rotation speed (rpm)	2	2
Gas flow (Nm³/h)	450 000	610 000
Air flow (Nm³/h)	430 000	575 000
Gas temperature in (C°)	375	375
Gas temperature out (C°)	120	140
Air temperature in (C°)	35	50
Air temperature out (C°)	325	324
Effectiveness, air side (%)	85.4	84.2
Effectiveness, gas side (%)	74.9	72.5

High pressure air and water or steam are frequently used as the medium for air preheaters cleaning. Cleaning devices based on those media help air preheaters to maintain their normal operation. In most cases, sootblowing devices are installed at the junction of the air preheater and the flue gas duct. Superheated steam or dry air via high pressure nozzles is used to periodically clean the heating surface elements. Additionally, permanent water wash piping is also installed to clean the air preheater of heavy ash deposits. The water wash piping is typically located at the top of the rotor, so that most heating surface elements can be exposed to the nozzles while rotation.

1.2.3 Concerns with Air Preheaters

The reason that air preheaters are equipped with cleaning means is the main issue of air preheater fouling. Fouling involves deposition of substances such as sulfuric acid, as well as ash deposition.

In the case of acid deposition, SO_2 is partly converted into SO_3 at the boiler back-end. Subsequently, SO_3 and moisture form sulfuric acid (H_2SO_4). Most air preheaters are operated at minimum metal temperatures larger than the H_2SO_4 acid dew point, to avoid sulfuric acid condensation onto the metal surface. If not mitigated, this can lead to air preheater cold-end layer corrosion.

One new form of air preheater fouling and corrosion has become an issue with the penetration of SCR's to the coal-fired power plant fleet. When SCR is used upstream of the air preheater, ABS fouling becomes a serious issue that needs to be addressed by power plant operators.

1.3 Ammonium Bisulfate

1.3.1 ABS Formation

In the SCR process, some ammonia would pass the SCR reactor unreacted. Some of the ammonia slip would combine with sulfuric acid (H_2SO_4) and/or sulfur trioxide (SO_3) to produce ammonium sulfate ((NH_4)$_2SO_4$) and ammonium bisulfate (NH_4HSO_4). The global

NH_3-SO_3 reactions that take place in the formation of these salts are [9]:

$$2NH_3 + SO_3 + H_2O \leftrightarrow (NH_4)_2SO_4 (s) = \text{Ammonium sulfate (AS)}$$

$$NH_3 + SO_3 + H_2O \leftrightarrow NH_4HSO_4 (l) = \text{Ammonium bisulfate (ABS)}$$
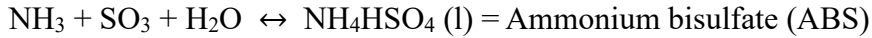
These reactions proceed as the flue gas is cooled down in the air preheater.

At the typical gas and metal air preheater temperatures, $(NH_4)_2SO_4$ exists as solid in the flue gas. Formation of $(NH_4)_2SO_4$ should not present a problem then, since the solid can not adhere to the air preheater metal surfaces as readily as a condensed phase [9]. However, NH_4HSO_4 deposits as sticky liquid and it can result in serious fouling and plugging problem. Plugging is used to characterize an excessive case of fouling, where the deposit plugs the open space in the air preheater basket, forcing the draft balancing system of the unit (forced and induced fans) to exceed their maximum capacity, forcing a shut down for water washing of the air preheater, with the associated down time and lose of generation.

Typically, the flue gas enters the air preheater around 650°F, and leaves around 250°F. A temperature profile along the air preheater is presented in Figure 6. It is reported that ABS deposit is usually found at the cold and intermediate air preheater layers where the temperature is approximately 315°F [6]. The temperature at which ABS starts forming along the decreasing air preheater temperature profile is called ABS formation temperature, or ABS initial formation temperature. During the heat transfer cycle of the air preheater, the

temperature of the heating elements changes as they are continuously exposed to hot flue gas and cold combustion air. When the metal temperature is lower than ABS formation temperature, ABS will deposit on the heating elements. It is reported that in most air preheaters, ABS deposits are observed down-stream of the anticipated dew point, or formation temperature [6].
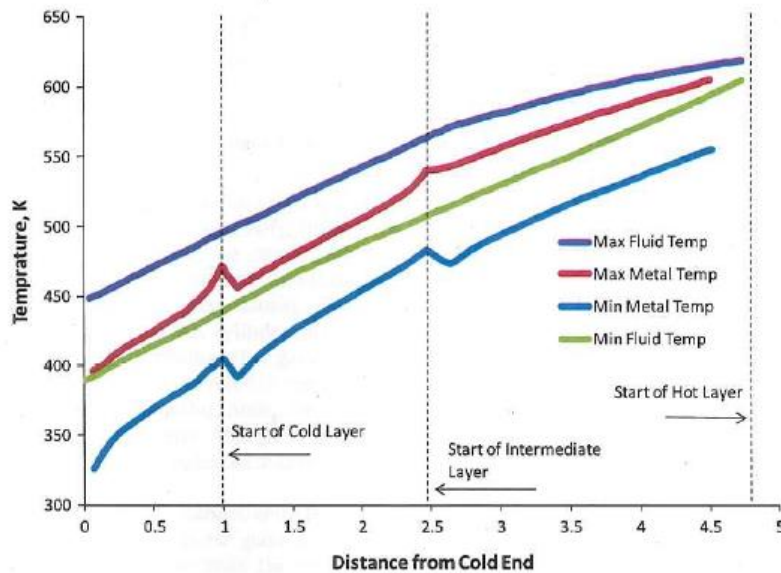
Figure 6. Typical Metal and Fluid Temperature Profile in the Air Preheater [6]

1.3.2 Discussion of Problem Due to ABS Fouling

During the ABS fouling process, ABS firstly forms and deposits onto the cold and intermediate layers of the air preheater. Subsequently, fly ash in the flue gas would adhere to the heating surface element. Gradually, it can cause a serious fouling issue. This fouling issue would result in increased air preheater pressure drop and associated thermal efficiency deterioration. If the pressure drop becomes significant, the boiler must reduce

load, leading to an inevitable unit outage.

ABS fouling is a significant problem when the ABS deposit accumulates at the intermediate layer. Some of the reasons for this are:

(1) Different from the cold-end layer, the intermediate layer is always manufactured from light-gauge carbon steel which is easy to be corroded due to the ABS deposits;

(2) Since the sootblowing equipment is located at both ends of the air preheater, the intermediate layer ABS deposit is difficult to be removed by sootblowing;

The key factors contributing to ABS fouling can be classified into two parts: the NH_3 and SO_3 concentration, and the air preheater design characteristics [2]. The concentration of NH_3 and SO_3 in the flue gas directly impacts the ABS formation temperature, as shown in Figure 7. Figure 7 shows an ABS formation temperature map developed by Hitachi-Zosen using thermodynamic equilibrium calculations [2]. As shown in Figure 7, higher concentrations of NH_3 and SO_3 will result in higher ABS formation temperatures. A high ABS formation temperature means that the ABS will form far away from the cold end, into the hotter parts of the air preheater, which is very difficult to be cleaned by sootblowing. On the contrary, low concentrations of NH_3 and SO_3 would lead to low ABS formation temperatures which will be more adequate for fouling-free air preheater operation. Therefore, concentration of NH_3 and SO_3 in the flue gas is strictly limited to avoid the ABS fouling issue. References

prescribe NH_3 and SO_3 concentrations, to prevent ABS fouling, in the range of 0-2 ppm [2].
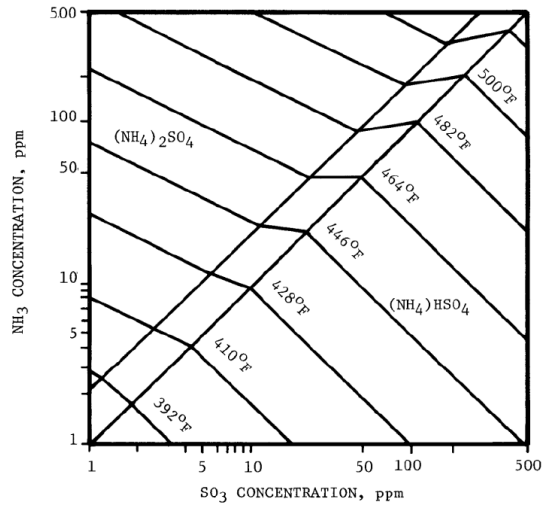
Figure 7. Hitachi-Zosen Map of Formation Temperature of Ammonia Bisulfate [2]

There are some main factors that lead to high concentration of NH_3 and SO_3. These include

for NH_3, the quantity and utilization effectiveness of the ammonia in the SCR, and SCR

catalyst performance. For SO_3, these include, the sulfur content in the fuel and the SO_2 to

SO_3 conversion effectiveness, as well as the SCR catalyst fly ash composition (vanadium

promotes oxidation of SO_2 to SO_3 in the SCR reactor). In addition to these factors, some

other factors can influence high NH_3 and SO_3 concentrations in the flue gas, and thereby

impact ABS formation. These factors include boiler operation which can impact high NO_x

formation and its level at the SCR inlet, and ash alkalinity (CaO, MgO) which impact SO_3

concentration indirectly.

The air preheater design characteristics is other major contributing factor to the ABS

fouling issue. The three major influencing design factors are: the element profile, air preheater basket layer depth and configuration, and basket material selection.

There are two typical types of element profiles in air preheaters, close and open. Closed element profiles have no flow communication between channels. The Double Undulated (DU) element is an example of an air preheater open element profile. In this profile the flow can move across the element between two sheets. Generally, the closed profile has better ABS fouling resistance performance, since the flow energy from the sootblowers have less deposit shattering energy waste than in the open profile.

The depth of the heating element layers directly affect the temperature profile along the flow direction, thereby influencing the ABS formation location in the air preheater. As previously discussed, intermediate and cold layers have a higher risk of ABS fouling. Deeper cold layers are better choice to mitigate ABS deposition occurring within a single layer. In regard to material selection, carbon steel is the most common material used for air preheater heating elements. However, fouling and acid attack can damage carbon steel. An enameled plate is typically employed to mitigate fouling of air preheater heating elements. Fly ash and other deposits are not easy to adhere on the enameled material. Therefore, it has been widely used for the cold layer in air preheaters with a risk of fouling and corrosion.

1.3.3   Mitigation of ABS Fouling in Air Preheaters

Based on the operating experience with SCR's in Japan, Germany and the United States for decades, a good deal of experience has been accumulated on the ABS fouling issue. A summary of air preheater fouling criteria, including potential mitigating approaches is provided in Table 2. It is the concensus that the most important factors for preventing ABS fouling are the control of excess SO_3 and NH_3. If SO_3 < 2-3 ppm and NH_3 < 1-2 ppm, the ABS fouling can be greatly avoided. However, it is not so simple to meet this goal.

Table 2. Air Preheater Fouling Criteria [2]

Fouling Factor	Criteria	Mitigation Options
SO_3	< 2-3 ppm > 2-3 ppm	● OK ● Related to fuel quality and/or catalyst activity in SCR application ● Add limestone to coal
NH_3	< 1-2 ppm > 1-2 ppm	● OK ● Monitor catalyst activity ● Replace/add catalyst ● Reduce reagent injection
Element Layer Split	● Shallow cold/int. layer ● Deep cold/int. layer ● Deep cold-end layer	● Less desirable ● Better ● Best (all deposition within single layer)
Element Material	● Carbon steel ● LACR ● Enamel	● Poor (corrosion) ● Better ● Best (lowest depositon/corrosion)
Element Profile	● Open ● Closed	● Less desirable ● Better cold-end sootblower penetration/water washing
Cold-End Sootblower	Rapid fouling if malfunctioning or out of service	● Upgrade nozzle to high-energy design ● Consider spare
SCR Location	● High dust ● Low dust	● Lower fouling ● Higher fouling

1.4 Scope of This Study

It has been discussed that ABS is an acidic deposit that forms on the metal elements of air preheaters in utility boilers. Because of the sticky nature of ABS, particles in the flue gas stream accumulate on the ABS wetted surface and aggravate fouling, leading to plugging of the air preheater [6]. Although fouling mitigation approaches have been proposed and proven with success, an important aspect of ABS formation and its detrimental impact on boiler operation is the ability to monitor ABS formation temperature. If information on ABS formation temperature could be readily available, the ABS deposition location could be identified. Subsequently, corresponding actions to avoid further fouling could be taken by boiler operators.

In this study, a literature review is provided, including previous studies of ABS formation temperature determination, by modeling and experimentation. Information on a sensor employed to measure ABS formation temperature in the field is introduced as well. An ABS modeling effort is then undertaken. This modeling is based on field data using plant performance data and readings from an ABS formation temperature monitor. PCA and SA were applied to reduce the number of variables that are important to impact ABS formation temperature. Then, KMC was used to select representative data samples. NN and SVM were employed to develop ABS formation temperature models.

These models were assessed in their ABS formation temperature predicted capabilities. An approach was finally recommended for a soft sensor for ABS formation temperature estimation based on SVM and NN. It was found that the prediction accuracy of this approach is within 8.8% of the ABS formation temperature determined by an actual ABS probe installed at a coal-fired power generation unit.

2 LITERATURE REVIEW

2.1 Previous Studies of ABS Formation Temperature

Studies on ABS formation temperature modeling have been carried out and reported in the literature. Examples of ABS formation temperature models are those from Radian [6][12], Hitachi-Zosen [2], Matsuda [11], and Menasha [6]. Most of model predictions of ABS formation temperature are related to the product of the concentration of NH_3 and H_2SO_4. One example of such relationship is shown in Figure 8. In Figure 8, model results and experimental data for ABS formation temperature are reported vs. the product, $[NH_3]*[H_2SO_4]$. The Radian model and the Hitachi-Zosen model provide a relatively lower ABS formation temperature than the corresponding temperatures obtained and reported by Mensha and Matsuda. The details of these four classical models are introduced next.
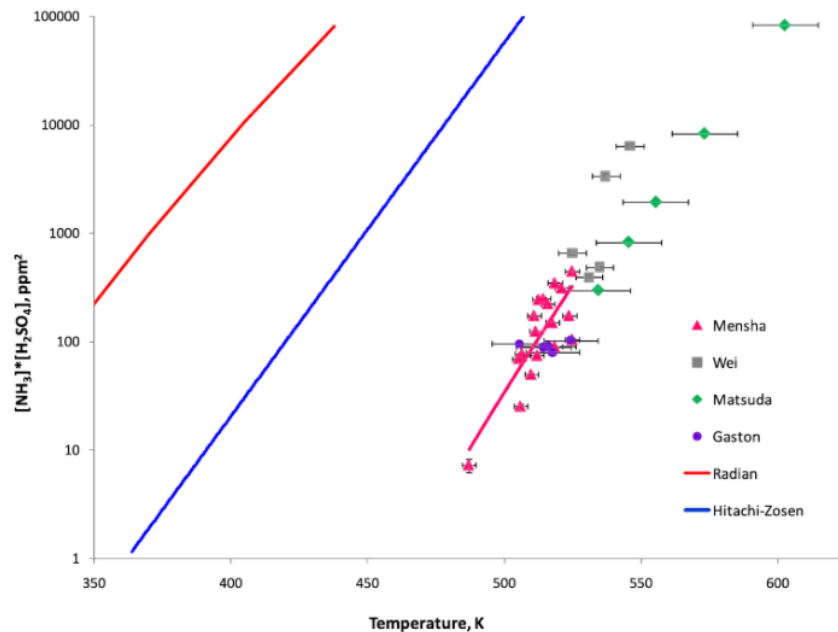
Figure 8. Results of Previous Studies of ABS Formation Temperature [6]

2.1.1 Radian Model [6] [12]

One of the earliest studies of ABS formation temperature is provided by Radian. Radian utilized results from various power plants to develop a kinetic model for the predition of ABS formation temperature and deposition of ABS. The Radian work identified the following principal chemical reactions for the formation of ABS:

$NH_3+SO_3+H_2O \rightarrow NH_4HSO_4$

$NH_3+H_2SO_4 \rightarrow NH_4HSO_4$

$SO_3+H_2O \rightarrow H_2SO_4$
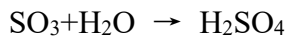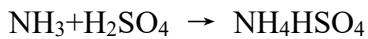
An equation was proposed to rate the formation of ABS in air preheaters according to [9]:

Radian Number = $[SO_3] \times [NH_3] \times [T_{IFT}] \times [T_{rep}]$

Where T_{IFT} is the initial ABS formation temperature, T_{rep} is a combination of exit flue gas temperature and cold-end metal surface temperature, SO_3 and NH_3 are sulfur trioxide and ammonia concentrations in the flue gas. A larger Radian number indicates a higher probability for ABS formation [12].

In the Radian study, the conversion of SO_3 to sulfuric acid was considered very important since the conversion of SO_3 could reduce the amount of SO_3 available in the flue gas to react directly with NH_3. Therefore, it could lead to low ABS formation temperature because of the low reactant concentrations. As shown in Figure 8, the ABS formation temperatures predicted by the Radian model are relatively lower than those reported by the other studies.

Menasha reported that real ABS deposits are typically and mostly observed at temperatures located down-stream of ABS formation temperatures and predicted by theoretical calculations [6]. These down-stream ABS deposits location temperatures would then validate the predictions of ABS formation temperatures from Radian.

2.1.2   Hitachi-Zosen Model [2]

Hitachi-Zosen studied the formation of ammonium bisulfate and ammonium sulfate, theoretically. The formation temperature predicted by Hitachi-Zosen is included in Figure 7. These Figure 7 predictions are based on thermochemical calculations, not experimental work. The data in Figure 7 were re-plotted in Figure 8 with the other ABS formation temperature data. The Hitachi-Zosen model also predicts relatively low ABS formation temperatures.

2.1.3   Matsuda Model [11]

Matsuda designed experiments to study ABS formation temperature. A diagram of Matsuda's experimental apparatus is presented in Figure 9 [11]. In this setup a gas mixture containing different amounts of NH_3 and SO_3 was passed through a glass tube reactor in a furnace, with a decreasing temperature gradient. The furnace temperature decreased along the axial direction from 680 to 210°F. Eight axial zones were divided in the glass tube and a quartz wool was fitted along the glass tube to let ABS deposit on it. The approximate

midpoint temperature of the zone with the most dominant deposit was defined as the ABS

formation temperature at the corresponding NH_3 and SO_3 concentration. Five experiments

were performed using a gas mixture containing NH_3 and SO_3 by the following respective

amounts 833: 100, 83.3: 100, 83.3: 10, 30: 65, 30: 10 (units in ppm). Matsuda indicates

that $NH_3 + H_2SO_4 = NH_4HSO_4$ is the predominant reaction below 570°F. Based on this

assumption, Matsuda reported that the vapor pressure of ABS can be expressed as:

$P_{NH_3} \cdot P_{H_2SO_4} = 1.14*1012 \exp(-53000/RT)$ (P in atm).

Where R is an ideal gas constant, and the value of this constant is 8.314 $J \cdot mol^{-1} \cdot K^{-1}$. T is a

mixed gas temperature.
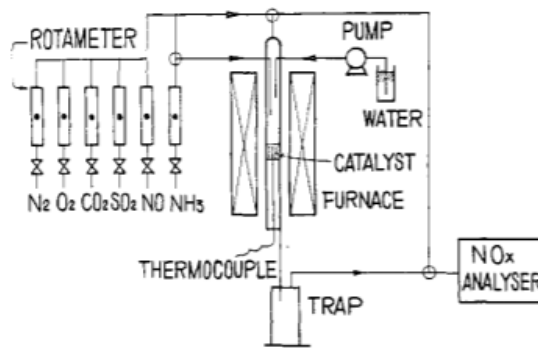
Figure 9. Matsuda's Experimental Design [11]

2.1.4   Menasha Model [6]

Menasha developed an experimental model, based on the experimental design shown in

Figure 10. In Menasha's experiments, simulated flue gas was composed of 75% N_2, 13.5%

CO_2, 8% H_2O, 3%O_2, 400ppm SO_2, 2-10ppm NH_3, and 5-45ppm H_2SO_4 [6]. Nitrogen was passed through a liquid SO_3 cylinder, preheated and then mixed with the other gases before entering the test channel. Cool, compressed air was introduced in the channel for counterflow cooling. Along the channel, temperature changed nearly linearly, and almost all the SO_3 converted into H_2SO_4. The wall temperature was used to determine ABS formation temperature. The experimental results found that ABS forms as aerosol and then migrates to the wall surfaces of the channel. Menasha's results are at a relative low $[NH_3]*[H_2SO_4]$ region, as compared to Matsuda's results. The results of Menasha and Matsuda confirm each other, since they have similar temperature gradients so close to each other.
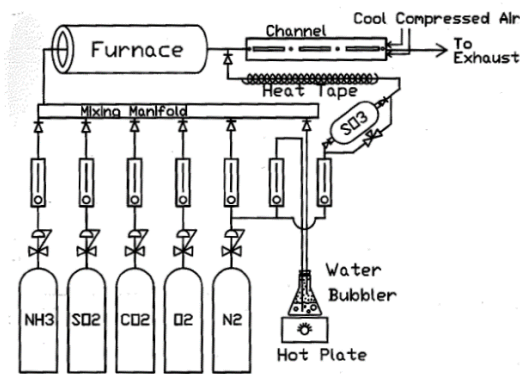
Figure 10. Menasha's Experiment Design [6]

From Figure 8, it can be seen that the Radian model and the Hitachi-Zosen model (two of the earliest models, based on thermochemical calculations) give relatively lower ABS formation temperature compared to other models. The predictions of Menasha, Matsuda, Wei and Gatson are close to each other, at a higher ABS formation temperature. All the

models provide predictions related to $[NH_3]*[H_2SO_4]$. It should be noticed that the concentration of H_2SO_4 is pretty difficult to measure in power plants.

2.2 Measurement of ABS Formation Temperature

In this study, data from an ABS fouling probe from Breen Energy Solutions, were used to obtain ABS formation temperature used in the modeling effort. The probe was installed at the air preheater inlet to measure ABS formation temperature and ABS evaporation temperature. The probe can control temperature of the detector's heating surface by application of cooling air [12]. A simplified diagram of the Breen ABSensor is shown in Figure 11.

At the beginning of a measurement cycle, the tip temperature is high enough and there is no material condensed on it. Then, the tip temperature is varied as cooling air flow is increased. When the temperature of the tip is sufficiently low, material begins to condense on the tip and an electric current is recorded by the device. The corresponding temperature for this point is noted as the "ABS Formation Temperature". After this step, the cooling air to the tip is reduced and the tip temperature begins to rise. As the temperature increases, ABS starts to vaporize and finally it vanishes from the tip. This temperature is recorded as the "ABS Evaporation Temperature".
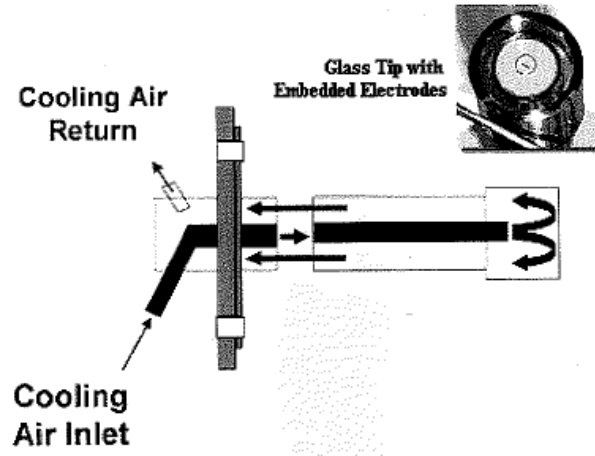
Figure 11. Breen AbSensor - Condensables Measurement Device [21]

3 MODELING

3.1 Plant and Data Description

Data used in this study were obtained from Cayuga Unit 1. Cayuga Unit 1 is a 160 MW unit with a tangentially-fired boiler equipped with low NO_x burners and overfire air for NO_x emissions control. The unit was retrofitted with an anhydrous ammonia-based SCR system. The unit experienced heavy ABS fouling of the air preheater, resulting in an average of four air preheater water washes per year. In addition to this side problem, the cost of anhydrous ammonia represents a heavy burden on the operating cost of the SCR system [13]. The station was interested in keeping a good handle on their NH_3 operation to reduce NH_3 costs and minimize or eliminate the ABS fouling problem. Cayuga retrofitted the ABS probe from Breen Energy and performed an optimization of its boiler and SCR system. Cayuga Unit 1 field data were gathered for one month for analysis and modeling in this study.

The Cayuga data are composed of 14,230 samples, distributed in 49 variables including ABS formation temperature. The variables in the Cayuga data set are shown in Table 3. Some of variables may have multi-values, since there are redundant sensor measurements. For this reason, the 49 included variables led to 80 input parameters in total. ABS formation temperature models were set up to predict ABS formation temperature based on the Cayuga

data. ABS formation temperature was regarded as a single output of the model. All the remaining 48 variables (79 parameters) were used as input to the models.

Table 3. Variables in Cayuga Data Set

General Parameter:
Net MW   Gross MW   Fouling Evaporate Temp.   Fouling Formation Temp.   Main Steam Temp.   Total Air Flow
Furnace: Furnace Pressure
Superheater：   Steam Desuperheating Flow Low Range
Reheater: Desuperheating Flow Low Range   Primary Reheater Outlet Draft   Reheater Outlet Temp.
Economize: Inlet Draft   Outlet Draft   Outlet Gas Temp.   Outlet Damper Position   Bypass   Damper Position   Oxygen
SCR: Inlet: Temp. NO_x Diverter Position   Outlet: Temp.   Oxygen NO_x Dilution Skid NH3 Vap Temp   Load Based NH_3 Flow, Calculated   Dilution Skid Ammonia Flow   Operator Entered Allowable NO_x Bias %
Air Preheater: Air: Inlet Temp.   Outlet Temp.   Gas: Outlet Temp.   Cold End Temp. Bias   Bypass Damper Position
Emissions: NOx Emission   Analyzer Inlet SO_2 Unit 1 SO_2 Flow   ABS1 Outlet SO_2 Flow   Stack 1 CO_2 Opacity
Mill & Fan: FD Air Flow   Unit 1 Inlet Gas Flow   Coal Feeder Flow   Mill Motor AMPS, Speed   PA Fan Flow, Temp.   Coal-Air Temp.   Windbox to Furnace Diff. Pressure   Overfire Air Flow

3.2 Modeling Strategy

The overall modeling strategy is shown in Figure 12. Initially, variables were reduced by experience. Through this process, repetitive or less influential variables were removed to eliminate noise during modeling. For example, variables reporting data upstream in the combustion process, such as pulverizer information, were eliminated from the data set.

PCA was applied to further reduce the variables in the reduced processed data set. SA was used to analyze the inputs' influence on the output, so that the influence of each variable could be better assessed, resulting in an additional variable vector reduction. PCA and SA processes helped with the reduction of data dimension. Low dimensional data is more conducive to the improvement of model accuracy.

The selected reduced data were divided into two parts, training data and testing data. Training data were set to be about 70% of the samples of the selected data, while testing data were composed of the remining 30%. Training data were used for modeling and testing data for model verification during model training.

Finally, to further reduce the site of the data set, KMC was used to select even more representative samples.

After the compression of variables and samples, NN and SVM were employed to build the different models. All the data, including training samples and testing samples were used at the end to test and evaluate model accuracy.
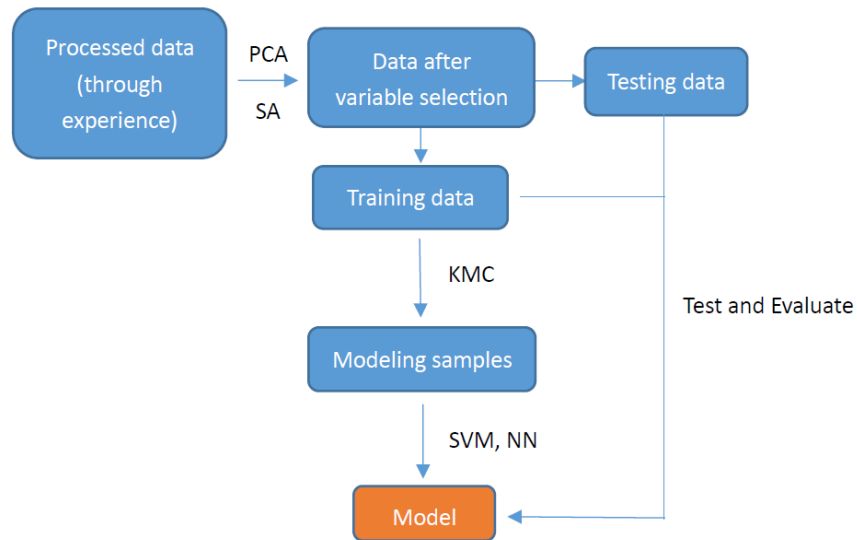
Figure 12. Overall Modeling Structure

3.3 Variable Selection

A variable selection process was carried out in two parts. In the first step, variables were reduced based on operational experience. For example, variables associated with the mills and fans are not pertinent nor play a direct role in the ABS formation temperature, thus, they were deleted to eliminate unwanted noise in the models. On the contrary, variables like SCR gas temperature and SCR inlet NO_x were preserved because they are highly related to the ABS formation temperature. Additionally, a filtering procedure was employed to discriminating abnormal values of the different variables. The criteria to eliminate

abnormal data were situations where the data were out of a reasonable range or remained unchanged over a period of time. After this step was implemented, 19 variables (25 parameters) were retained as shown in Table 4. Almost all the SCR and air preheater variables were retained because they are highly related to the ABS formation temperature. The second variable selection step used PCA. PCA was used to reduce the data dimension of the 19 variables.

Table 4. Fitted Variables

General parameter:
Net MW   Total Air Flow
Economize:
Outlet Gas Temp.   Oxygen
SCR:
Inlet: Temp. NO_x Outlet: Temp.   Oxygen NO_x Dilution Skid NH_3 Vap Temp   Dilution Skid Ammonia Flow Operator Entered Allowable NO_x Bias %
Air preheater: Air: Inlet Temp.   Outlet Temp. Gas: Outlet Temp. Cold End Temp. Bias   Bypass Damper Position
Emissions: NO_x Emission   Opacity

3.3.1   Principal Component Analysis

Principal component analysis is a statistical procedure that uses an orthogonal transformation to convert a set of observations of possibly correlated variables into a set of

values of linearly uncorrelated variables called principal components [14]. PCA can treat

high dimensional correlated data and is widely used for modeling of complex industrial

processes [12]. PCA can reduce the number of dimensions of data while it keeps a maximum

information of the raw data.

Mathematically, PCA transforms the original data to a new coordinate system so that the

greatest variance lies on the first coordinate (first principal component). The second

greatest variance lies on the second coordinate, and so on [15]. Consider a normalized matrix,

X with p columns (variables) and n rows (samples). Meanwhile, X has zero mean and unit

variance. The essence of PCA is a Karhunen–Loève (KL) transformation which can be

shown as:

$$X = PY \qquad\qquad (1)$$

$$\text{or } Y = P^T X \qquad\qquad (2)$$

Hence, Y is a projection of X which uses an orthogonal transformation P^T. Where the P

matrix is a p-by-p matrix whose columns are the eigenvectors of XX^T.

The covariance matrix of X can be defined as S_x. S_x can be expanded by the following

equation:

$$S_x = \frac{1}{n-1} X X^T \qquad\qquad (3)$$

XX^T itself can be recognized as proportional to the empirical sample covariance matrix of

the dataset X. Λ is the diagonal matrix of eigenvalues $\lambda(k)$ of XX^T,

$$\Lambda = PXX^TP^{-1} \tag{4}$$

The greatest eigenvalue $\lambda(1)$ in Λ represents the first principle component. After KL transforms, the first principle component can explain the $\frac{\lambda(1)}{\sum\lambda(k)}$ information of the original dataset X. Additionally, the first m principle components can represent $\frac{\lambda(1)+\lambda(2)+\cdots+\lambda(m)}{\sum\lambda(k)}$ information of X. For example, if the requirement is to keep 90% of X's information in Y. Once m satisfies $\frac{\lambda(1)+\lambda(2)+\cdots+\lambda(m)}{\sum\lambda(k)} > 90\%$, the data can be reduced to the m dimension by PCA. Therefore, PCA provides an effective way to reduce the dimensions of a data set. PCA was implemented by MATLAB in this study.

3.4 Sample Selection

The Cayuga data set contains over ten thousand samples. To obtain a more manageable data set, sample selection and compression was accomplished using KMC.

3.4.1   K-Means Clustering

KMC is a method of vector quantization, and it is popular for cluster analysis in data mining [16]. KMC is designed to divide M points in N dimensions into K clusters, so that the within-cluster sum of squares is minimized [17].

Mathematically, given a set of samples $(X_1, X_2, \ldots, X_m)$; where, each sample is a N-

dimensional real vector, K-means clustering tries to classify M samples into K ($\leq$m) clusters: S = {S$_1$, S$_2$, …, S$_K$}. Meanwhile, it also aims to minimize the within-cluster sum of squares (WCSS). WCSS is the sum of distance functions of each point in the cluster to the K center. In other words, K-means clustering attempts to meet:

$$\arg \min_{S} \sum_{i=1}^{K} \sum_{X \in S_i} ||X - \mu_i||^2 \tag{5}$$

where μ_i is the mean of points in S$_i$.

A sample result of K-means clustering application in this study is visually shown in Figure 13. The x and y axis in the figure represent the first and second principle component of the processed data, respectively. The data could possibly have more than two-dimensions, but it is more convenient to show the space distribution of data points in a two-dimensional surface. In the left plot of Figure 13, all the data points (more than 12,000 points) are densely distributed in a two-dimensional surface. After the K-means clustering process, just 110 cluster center points are compressed from the over 12,000 points. All cluster centers are shown on the right plot as red points. The 110 cluster centers can cover the characteristics in the over 12,000 data points. KMC reduced the number of samples in the training data set of this study, and improved data structure. This was supposed to increase model accuracy and decrease computing time. KMC was implemented by MATLAB in this study.
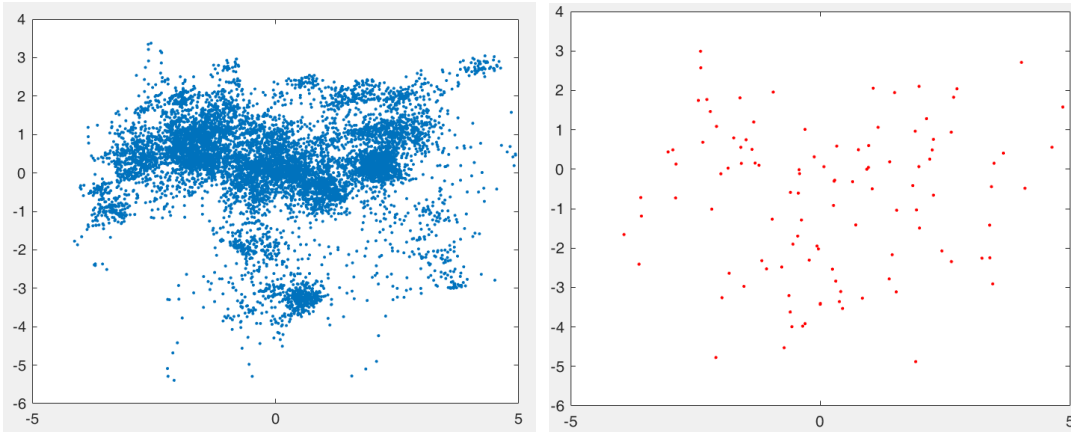
Figure 13. Example of K-means Clustering Application

3.5 Modeling Algorithms

3.5.1 Neural Networks

Neural network is a computational model used in computer science and other research disciplines, which is an imitation of the structure and function of the biological brain's neurons. As pictured in Figure 14, each individual neural unit connects with all the other adjacent layers' neural unit, and each unit computes using a summation function. Neural networks can consist of single or multi-layer architectures, where the end signal travels from the input layer to the output layer of the neural units.

If the training data have been taken as $\{(X_1, Y_1), ..., (X_L, Y_L)\}$, where X_i (i=1, 2, …, L) is the ith input vector and Yi (i=1, 2, …, L) is the ith output vector. Mathematically, a neural network problem can be interpreted as:

$$\overline{Y_i} = f(\overrightarrow{X_i} \cdot v + b) \cdot w \tag{6}$$

Where v is a weight vector, b is an offset, and f is a transfer function which minimizes

$$\sqrt{\sum_{i=1}^{L}(\overline{Y_i} - Y_i)^2}.$$ (7)

In this study, a neural network software called Neuframe [22] was employed to build the neural network models.
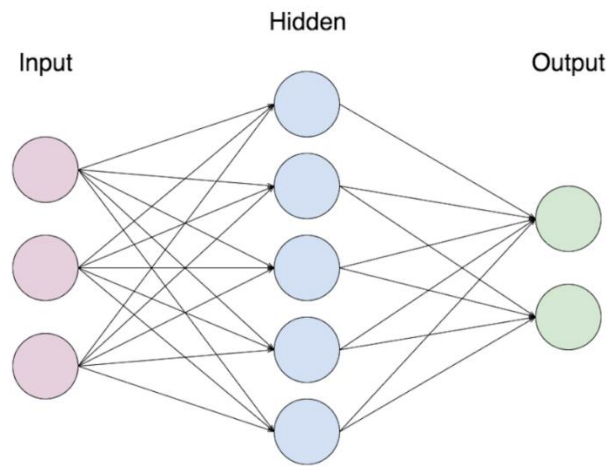
Figure 14. Neural Network Schematic

3.5.2 Support Vector Machine

Support vector machine is a novel machine learning method and it is a powerful tool for small sample problems [12]. SVM applies the structural risk minimization inductive principle to obtain good generalization on a limited number of learning patterns [18]. SVM is a widely-used algorithm in classification and regression analysis. Support Vector Regression (SVR) is the most common application of support vector machine. Compared to neural networks, SVM can easily avoid local minima and structure selection issues,

because SVM is based on the structural risk minimization principle, rather than the least

square methods or the maximum likelihood methods in traditional neural networks [12].

As indicated for neural networks, if the training data is $\{(X_1, Y_1), ..., (X_L, Y_L)\}$, where X_i

(i=1, 2, …, L) is the ith input vector and Yi (i=1, 2, …, L) is the ith output vector, in SVM,

a function f(x) needs to be found so that function f minimizes a given regularized risk

function. [12] That linear function f can be described in the form as below to formulate a

SVM problem [18]:

$$f(x) = <\omega, x> + b \tag{8}$$

Where ω is the weight vector, and b is the threshold and ω and b are identified by the

function f in the equation 8. Flatness in (8) means a small ω, and it requires to minimize

the Euclidean norm $||\omega||^2$. [18] If the Vanik's ε- insensitive lose function is employed, this

can be represented in an optimization way as [18]:

$$\text{Minimize } \frac{1}{2}||\omega||^2 + C \sum_{i=1}^{L}(\xi_i + \xi_i^*)$$

$$\text{Subject to} \begin{cases} y_i - < \omega, x_i > -b \le \varepsilon + \xi_i \\ < \omega, x_i > +b - y_i \le \varepsilon + \xi_i^* \\ \xi_i, \xi_i^* \ge 0 \end{cases} \tag{9}$$

The constant C>0, ξ_i and ξ_i^* are slack variables. The slack variables are variables that are

added to an inequality constraint to transform it to an equality. The ε- insensitive lose

function $|\xi|_\varepsilon$ is described by [18]:

$$|\xi|_\varepsilon = \begin{cases} 0 & if |\xi| < \varepsilon \\ |\xi| - \varepsilon & otherwise \end{cases} \tag{10}$$

By using a standard Lagrange multiplier and a dual set of variables, the SVM optimization

problem can be set up as: [12]

Maximize $\left\{ -\frac{1}{2}\sum_{i,j=1}^{L}(\alpha_i - \alpha_i^*)(\alpha_j - \alpha_j^*) < x_i, x_j > -\varepsilon\sum_{i=1}^{L}(\alpha_i + \alpha_i^*) + \right.$

$$\left. \sum_{i=1}^{L}(\alpha_i - \alpha_i^*)\,y_i \right\}$$

Subject to $\begin{cases} \sum_{i=1}^{L}(\alpha_i - \alpha_i^*) = 0 \\ \quad 0 \le \alpha_i, \alpha_i^* \le C \end{cases}$ (11)

Where α_i^* and α_i are Lagrange multipliers and K is the kernel function [12]. For instance

a Gaussian kernel is the most common kernel in SVM. After getting α_i^* and α_i by some

optimization algorithm such as sequential minimal optimization, the regression function

can be rewritten as: [18]

$$f(x) = \sum_{i=1}^{L}(\alpha_i^* - \alpha_i)\,k(x_i, x) + b \tag{12}$$

SVM was implemented by MATLAB in this study.

3.6 Sensitivity Analysis

After NN and SVM models were developed a sensitivity analysis was performed.

Sensitivity analysis is a study of how the uncertainty in the output of a model (numerical

or otherwise) can be apportioned to different sources of uncertainty in the model input [19].

In this study, a sensitivity analysis was used to test the influence of 25 inputs on the output

(ABS formation temperature). At first, a new sample was made up of the average of each

input. Then, one of the input was changed from its minimum value to its maximum value,

while other inputs were fixed at their average value. Through model prediction, the impact

on ABS formation temperature was associated with change in the corresponding inputs.

This process was repeated for all the inputs, and a better understanding of their effect on

ABS formation temperature were clearly identified. Some inputs were then eliminated for

subsequent modeling, since they had a second order contribution to the output.

4. RESULTS AND DISCUSSION

In this study, five models were built base on NN or SVM. The overview of each model is presented in Table 5.

Table 5. 5 Model Characteristics

Model	Initial Data Set	Data Processing Methods	Model Data Input	Modeling Method	NRMSE
1	14,230 samples 25 inputs	PCA, KMC	213 samples 10 inputs	NN	44.2%
2	14,230 samples 25 inputs	PCA, KMC	213 samples 10 inputs	SVM	19.6%
3	14,230 samples 25 inputs	SA, KMC	774 samples 7 inputs	SVM	13.6%
4*	12,717 samples 25 inputs	SA, KMC	849 samples 7 inputs	SVM	9.1%
5*	12,717 samples 25 inputs	SA, KMC	369 samples 4 inputs	SVM	8.8%

Notes:

4* 5*: Only full-load data in the initial data set;

NRMSE: Normalized Root Mean Square Error.

To test the accuracy of the models, a Normalized Root Mean Square Error (NRMSE) was used as the validation criterion. NRMSE is calculated as:

$$\text{NRMSE} = \frac{\sqrt{\frac{\sum_{i=1}^{n}(x_{pi}-x_{ai})^2}{n}}}{x_{a\ max}-x_{a\ min}} \tag{13}$$

Where n is the sample size. Additionally, x_a is the actual ABS formation temperature, and x_p is the predicted ABS formation temperature. $x_{a\,max}$ and $x_{a\,min}$ represent the maximum and minimum ABS formation temperatures among all samples.

4.1 Description of Model 1

Model 1 is based on a data set composed of 14,230 samples and 25 inputs (distributed in 19 variables). For this model, a normalization procedure was applied to the data to meet the requirement of PCA (zero mean and unit variance). After normalization, PCA was used to achieve variable reduction. In the PCA process, ten principle components (new inputs) were retained to meet the goal of keeping more than 90% of the input information. The contribution of each component to the input information is shown in Table 6. KMC was then used to compress the sample set. KMC was able to reduce the data set to a new set composed of 213 samples compressed from the 9,606 training samples in the original data set. After applying the KMC, 213 samples and 10 inputs data were directly used to implement modeling by neural network. A diagram of Model 1 is shown in Figure 15. As introduced in the modeling strategy section, the testing and training data shown in Figure 15 correspond to the data sets used to develop Model 1 and subsequent testing of the accuracy of the model with an independent data set not used in the building or training of the model.

Table 6. Contribution of Each Component in PCA Model – Model 1

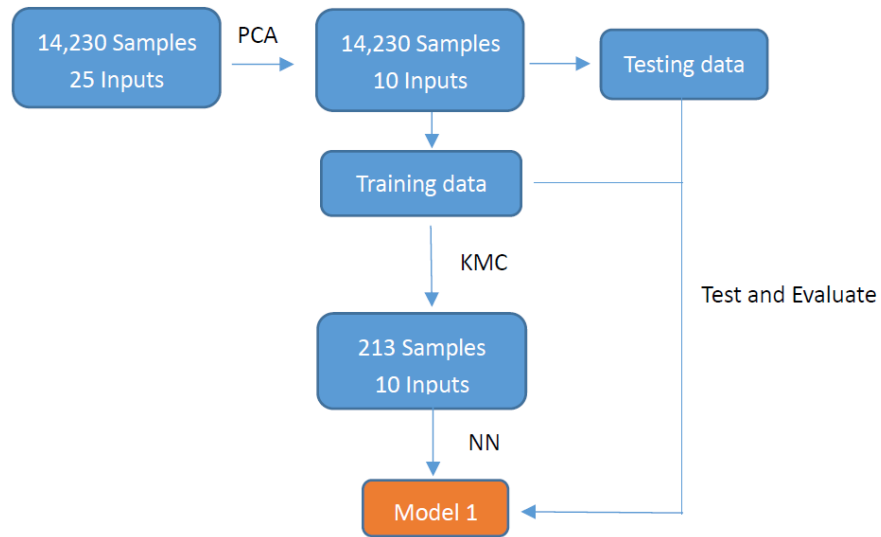| PCA Component	1	2	3	4	5	6	7	8	9	10	SUM
Data Contribution %	27.5	15.7	13.7	11.5	5.7	4.7	3.7	3.5	2.9	2.7	91.4

Figure 15. Diagram of Structure of Model 1

4.2 Description of Model 2

Model 2 uses the same 213 samples and 10 inputs selected by PCA and KMC in Model 1.

However, Model 2 is based on SVM, instead of neural networks. A diagram of the structure
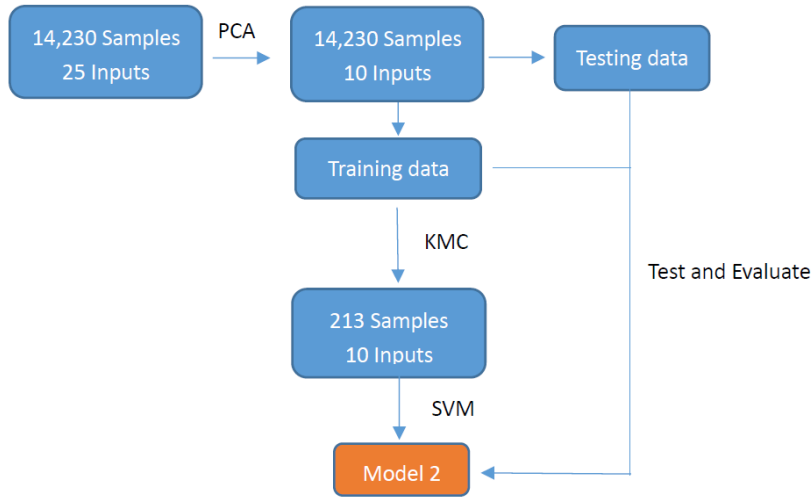
of Model 2 is shown in Figure 16.

Figure 16. Diagram of Structure of Model 2

4.3 Description of Model 3

For Model 3, a sensitivity analysis was used to help with variable reduction. By the use of this sensitivity analysis, the original 25 inputs were reduced to 7 inputs (distributed in 6 variables). Those variables include net load, SCR gas outlet temperature, SCR NO_x inlet concentration, dilution skid ammonia flow (2 inputs), dilution skid ammonia vapor temperature, and total air flow. SCR operating parameters such as temperature and ammonia injection are related to NH_3 slip as well as SO_2 oxidation to SO_3. Unit load and air flow relate to the residue time of flue gas in the SCR and further ABS formation timing. The variables were considered as the most relevant inputs in the 25 input set. Based on 14,230 samples and 7 input data, the data set for Model 3 was further developed using the process of KMC for later modeling with SVM. The PCA step was omitted for this model because the data is 7-dimensional instead of 25-dimensional, making dimensionality

reduction not highly needed. The diagram of the structure of Model 3 is shown in Figure 17.
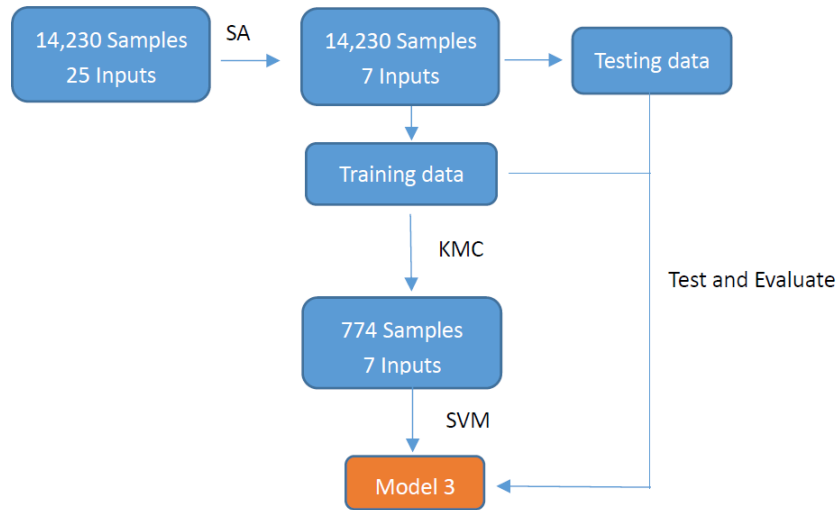

Figure 17. Diagram of Structure of Model 3

4.4 Description of Model 4

Different from the previous three models, Model 4 was based on only full-load data (>90% max-load). Except for the different data set used for development of this model, Model 4 was developed using the same approach as for Model 3. The structure of Model 4 is shown in Figure 18.
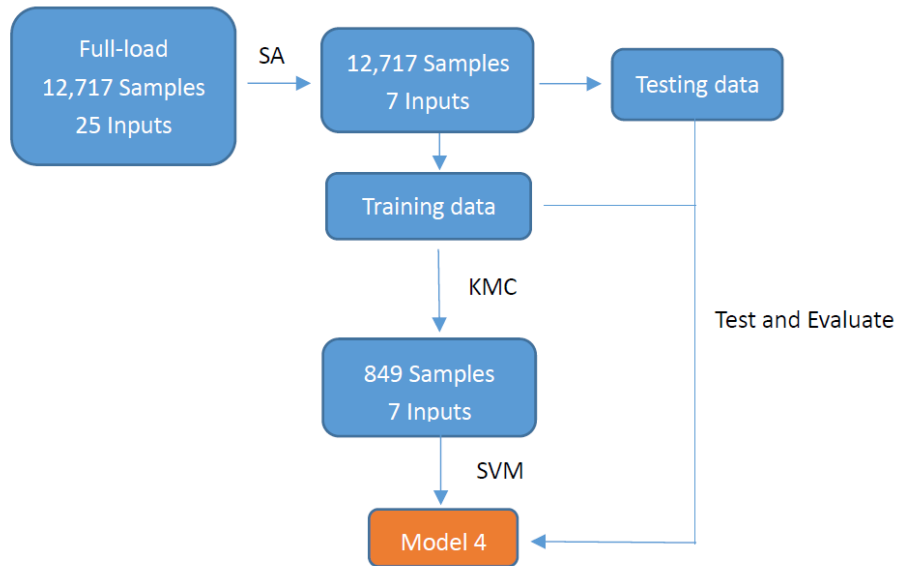
Figure 18. Diagram of Structure of Model 4

4.5 Description of Model 5

Four variables were selected to build Model 5. These variables are: SO_2 gas analyzer inlet concentration, SCR gas outlet temperature, SCR NO_x inlet concentration and dilution skid ammonia flow. These variables were chosen to find out if a reduced variable set could keep improve model accuracy in terms of predicting ABS formation temperature. As with Model 4, Model 5 was based on 12,717 data samples which correspond to full-load data. 12,717 samples were reduced to 369 samples through KMC, and SVM was again used to build Model 5. The structure of Model 5 is shown in Figure 19.
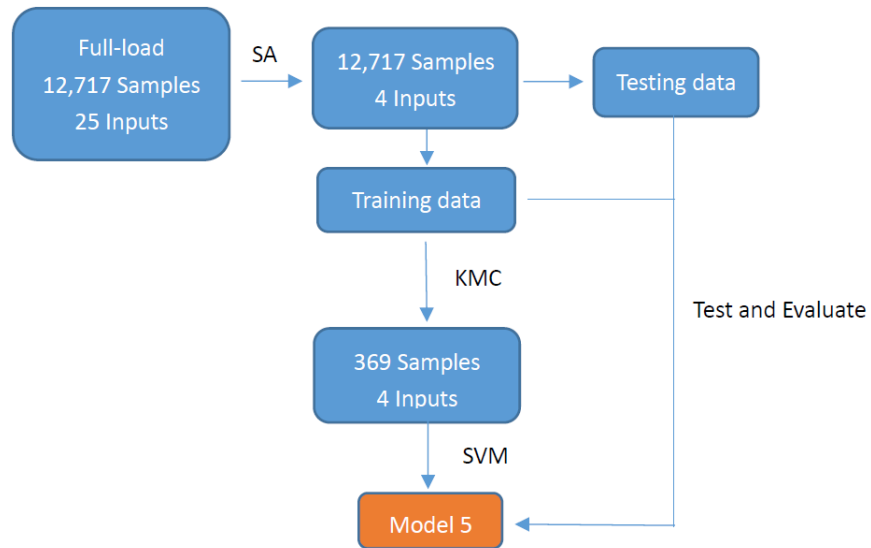
Figure 19. Diagram of Structure of Model 5

4.6 Models Results

Figures 20 to 29 provide results from the five different models. These figures include predicted vs. measured ABS formation temperature trending and estimations of statistical differences between the predicted and actual ABS formation temperature. NRMSE of 44.2%, 19.6%, 13.6%, 9.1%, 8.8%, for Models 1 to 5 were achieved. These NRMSEs were calculated from all the data samples, combining training and testing data used in each model.

As introduced in section 4.1, Model 1 was developed using neural networks and based on a data set of 14,230 samples and 25 inputs. The NRMSE of Model 1 is 44.2%. The results achieved with Model 1 are shown in Figures 20 and 21. It can be seen from Figure 20 that

the predictions of ABS formation temperature are not in line with the actual values. Additionally, Figure 21 indicates that Model 1 is not an accurate model to predict ABS formation temperature, since points on Figure 21 are not aligned along the perfect correlation that would be represented by the 45° line in the figure.

Model 2 uses SVM for modeling development, and it was based on the same data set of Model 1, 14,230 samples and 25 inputs. The NRMSE of Model 2 is 19.6%, which shows an improvement, compared to the result achieved with Model 1. The results of Model 2 are shown in Figures 22 and 23. Figure 23 shows that most of the predictions from Model 2 concentrate around 360°F with very insignificant sensitivity. Figure 23 shows that of ABS formation predictions in the middle temperature range from 340 to 390°F are relatively closer to the actual values than those samples outside this range. Both of these figures from Model 2 indicate that Model 2 is still not very good to reproduce ABS formation temperature based on the set of inputs for this model.

Model 3 was developed by SVM and based on 14,230 samples and 7 inputs. The NRMSE of Model 3 is 13.6%. As shown in Figure 24, Model 3 has a better tracking ability than Models 1 and 2. It was found that for 99% of data points, the deviation between the predicted and actual values in Model 3 are within 20°F of each other, as shown in Figure 25. Results from both the NRMSE and the two figures for Model 3 show an improvement

compared to the former two models.

Model 4 was developed by SVM and based on 12,717 samples and 7 inputs. Only full-load data were selected to develop Model 4. The NRMSE of Model 4 is 9.1%, which is a further improvement, as compared to Model 3. Figure 26 indicates that the tracking of ABS formation temperature in Model 4 is good. For more than 99% of the data points, the deviation between the predicted values and the actual values by Model 4 are within 15°F. However, it also can be found in Figure 27 that when the actual ABS formation temperature is below 340°F, Model 4 usually provides higher predicted values than the actual values.

Model 5 was developed by SVM and based on 12,717 samples and 4 inputs. Full-load data and less variables were selected to develop Model 5 to find out if a reduced variable set could help improve model accuracy. The NRMSE of Model 5 is 8.8%, which is the best accuracy achieved for all five models. Figures 28 and 29 show the performance of Model 5. Model 5 has a good tracking ability to the ABS formation temperature. At the same time, when the actual ABS formation temperature is below 340°F, Model 5 still provides a higher prediction of ABS formation temperature, as shown in Figure 29.

The accuracy of the models was sequentially improved from Model 1 to Model 5. Several conclusions can be drawn from comparing the five models:

First, comparing results between Model 1 and Model 2, it can be found that SVM has a better predictive accuracy for ABS formation temperature than that of neural networks. The NRMSE of Model 2 is about half of the Model 1. The reason for this phenomenon is that SVM is more suitable for small sample set modeling. Here, small sample set does not mean the number of samples, but the operating conditions encompassed by the samples. Although the Cayuga data set has more than 10,000 samples, many of the samples correspond to the same operating condition. Additionally, the main advantage of SVM is that it adopts the structure risk minimization (SRM) principle, which has been shown to be superior to the traditional empirical risk minimization (ERM) principle, employed by conventional neural networks [20].

Second, the accuracy of the prediction is further improved from Model 3 to Model 4, because only full-load data was selected to develop the Model 4. In the Cayuga data, more than 89% of the unit operating data were at full-load. The conditions at partial-load vs. full-load can be very different. Many uncertainties are avoided when full-load data is used for modeling. Full-load operation condition is also more stable, which is a benefit to improve model accuracy. This may imply that a large data set is needed to better model ABS formation temperature at part load together with additional variables. It should also be noted that it may be that the ABS temperatures produce by the actual probe are not reliable at part load.

Third, variable selection is very important for model development. By using PCA and SA, the inputs to the models were reduced from 25 inputs (Model 2) to 7 inputs (Model 3) and from 7 inputs (Model 4) to 4 inputs (Model 5). At the same time, the accuracy of the models was greatly improved. When variables highly relative to the ABS formation were chosen, the reduced variable set helped to improve model accuracy. Additionally, data dimension reduction can increase data density, and deletion of lower order variables can get rid of noise during model development.

Fourth, both Models 4 and 5 can not provide a good prediction when the ABS formation temperature is below 340°F, even though Model 4 and Model 5 have relatively high model accuracy. Insufficient data in this range may be the cause of the bad predictions at these temperatures, or the reliability of the ABS temperature probe at those lower temperature.
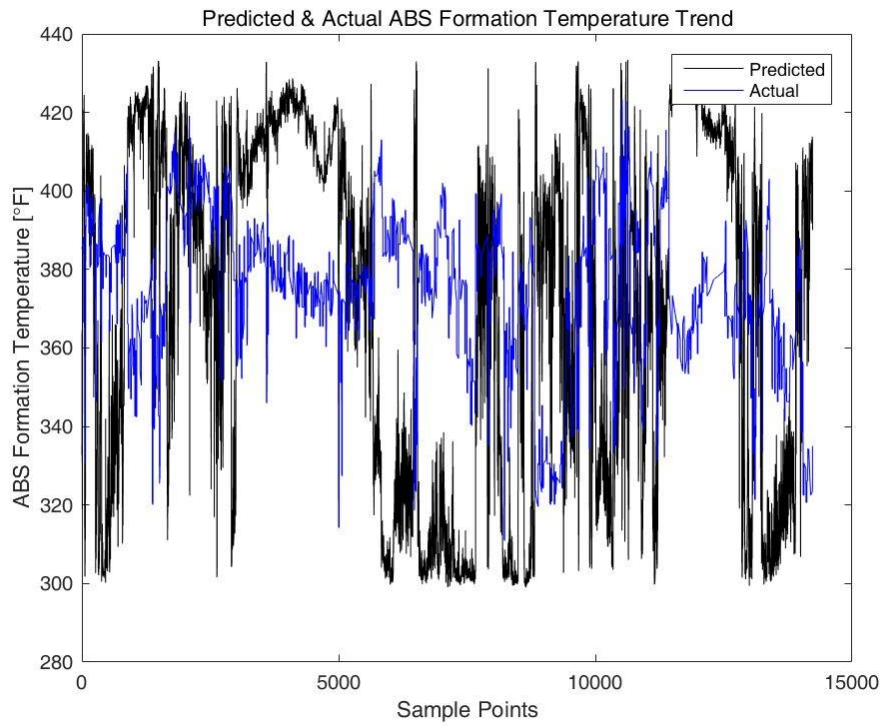
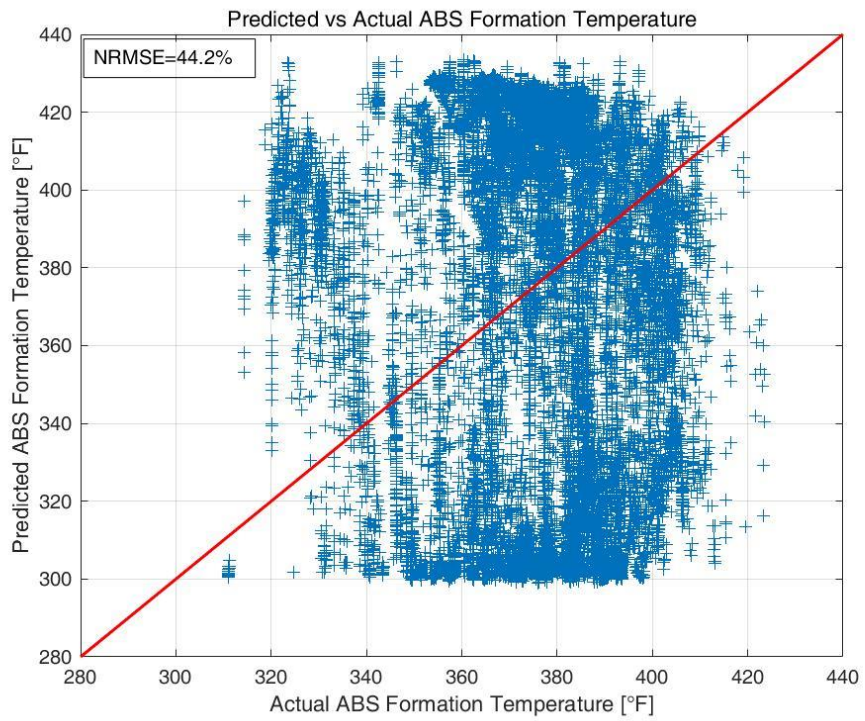Figure 20. Model 1 Results – Predicted and Actual ABS Formation Temperature Trend

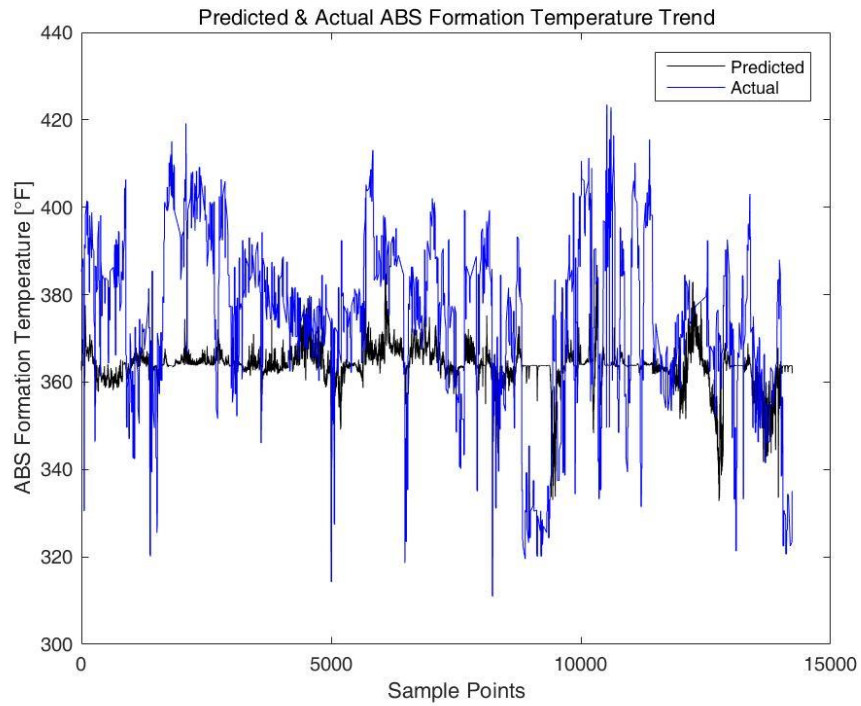Figure 21. Model 1 Results – Predicted vs. Actual ABS Formation Temperature

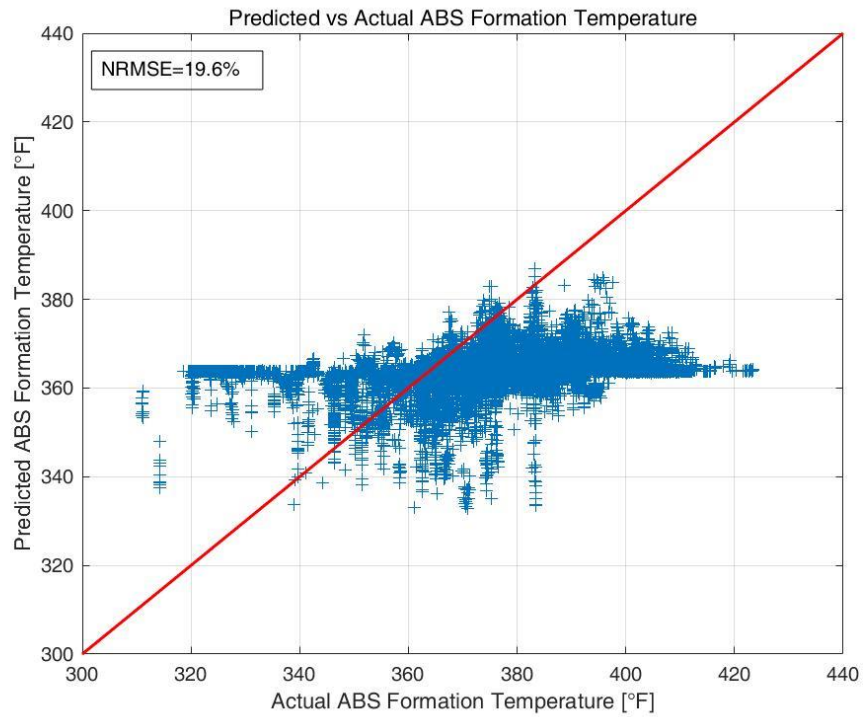Figure 22. Model 2 Results – Predicted and Actual ABS Formation Temperature Trend

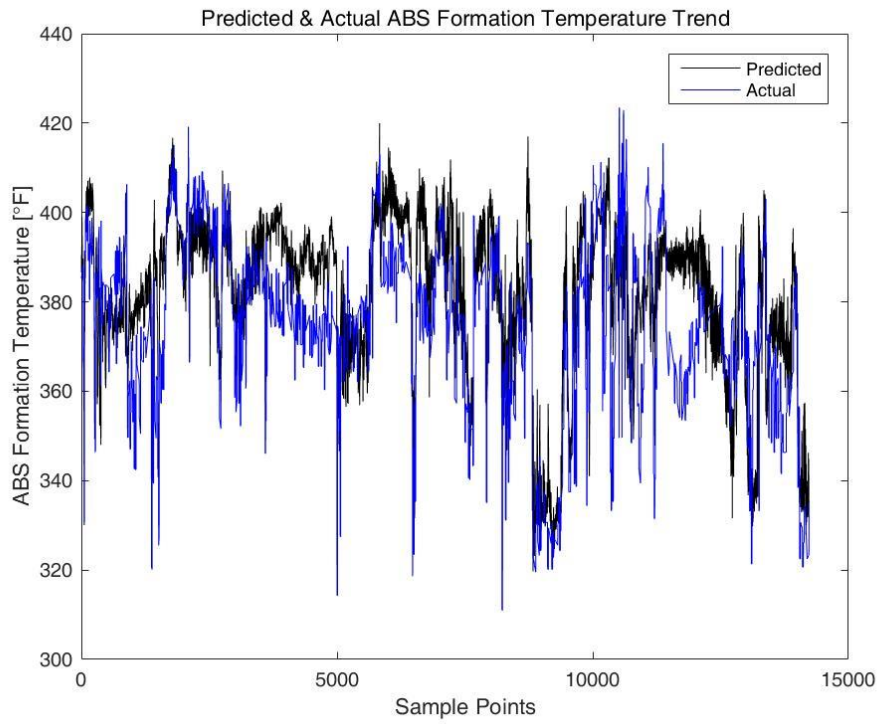Figure 23. Model 2 Results – Predicted vs. Actual ABS Formation Temperature

Figure 24. Model 3 Results – Predicted and Actual ABS Formation Temperature Trend
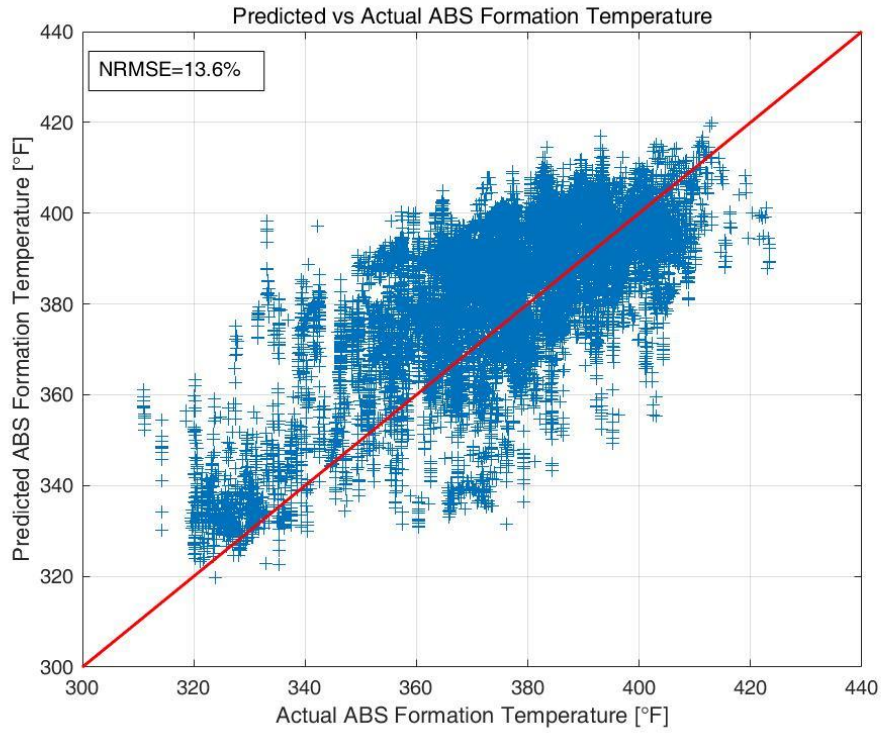

Figure 25. Model 3 Results – Predicted vs. Actual ABS Formation Temperature
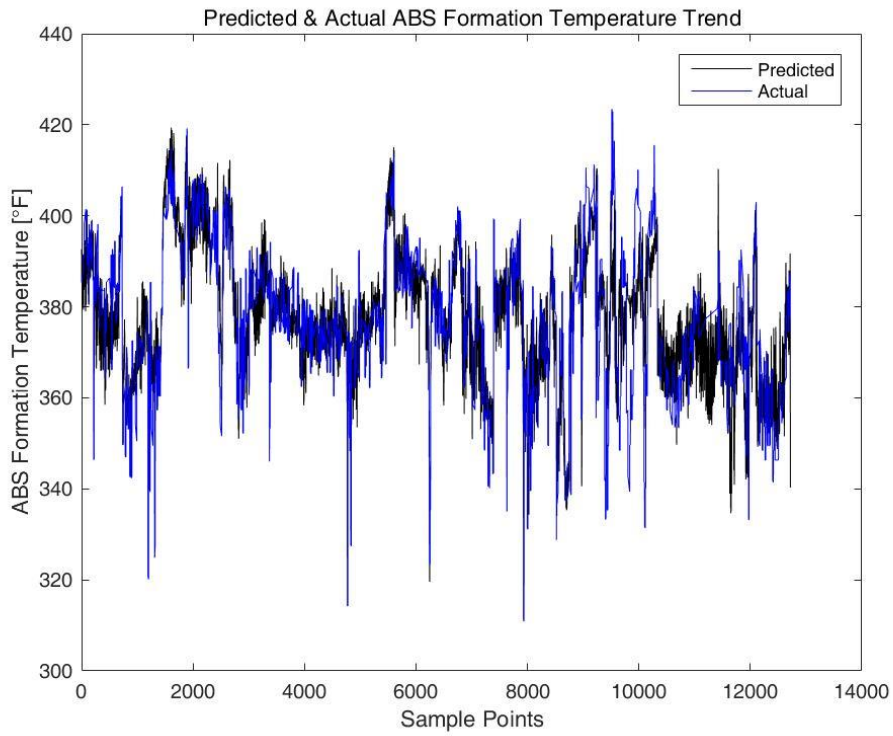
Figure 26. Model 4 Results – Predicted and Actual ABS Formation Temperature Trend
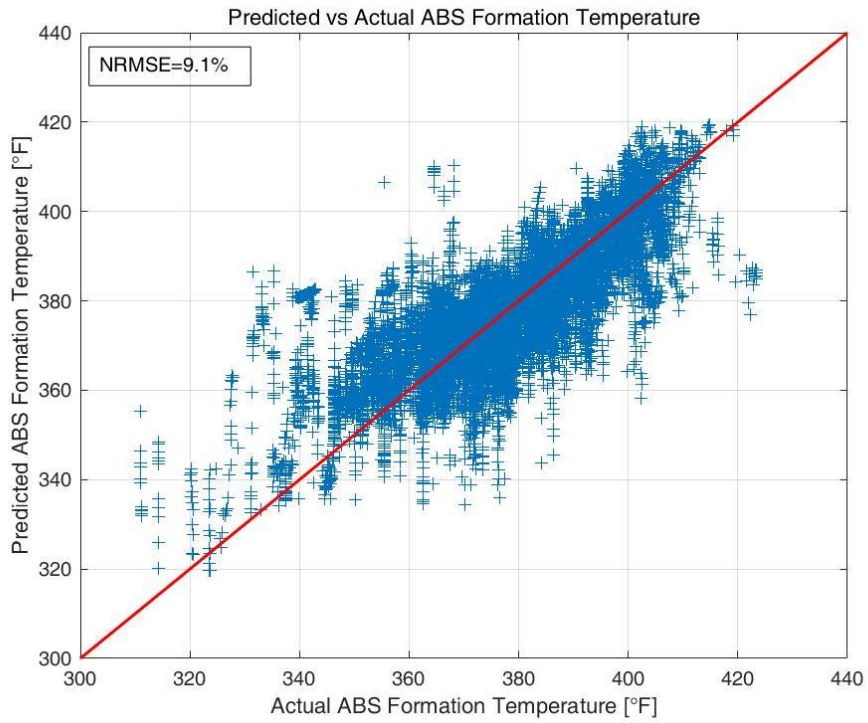

Figure 27. Model 4 Results – Predicted vs. Actual ABS Formation Temperature
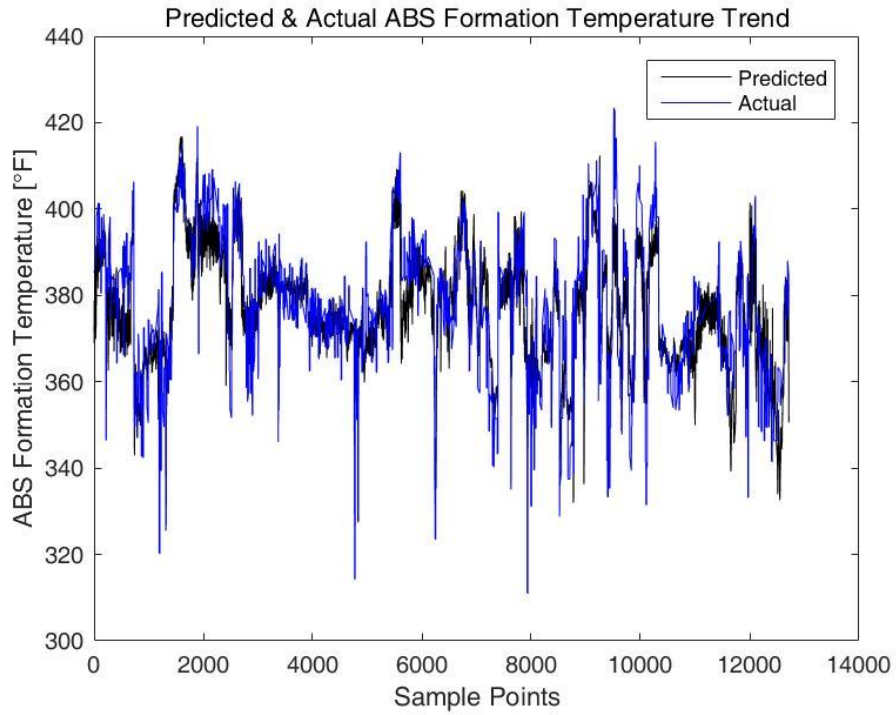
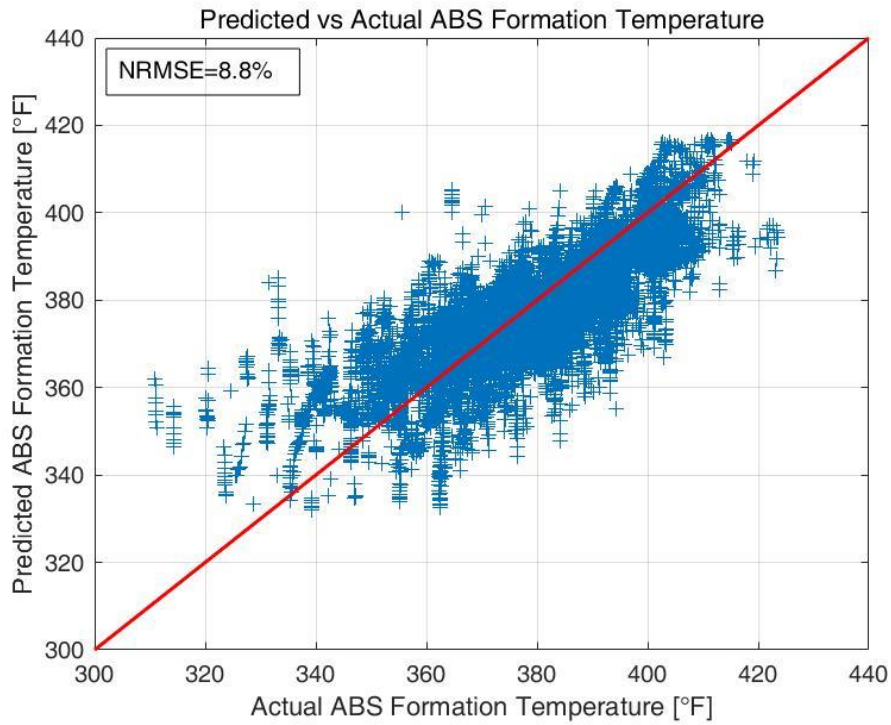Figure 28. Model 5 Results – Predicted and Actual ABS Formation Temperature Trend

Figure 29. Model 5 Results – Predicted vs. Actual ABS Formation Temperature

Both NN and SVM are data mining methods based on pure mathematical approaches such as the ERM principle or the SRM principle. Thus, these models do not contain elements based on the physical nature of the process they attempt to model. A model that would contain certain degree of first principles would be regarded as a more reliable model.

A sensitivity analysis was performed to assess the sensitivity of model output to certain input variables. Two inputs were analyzed in the sensitivity analysis, SCR gas outlet temperature and SCR inlet NO_x. In this sensitivity analysis, only these two variables were varied from their minimum to maximum values, with all the other variables fixed at their average values.

Results are presented in Figure 30 for Model 5. This is because it was the model that exhibited the best ABS formation temperature performance, as compared to the other four models. Figure 30 shows a direct correlation between SCR gas outlet temperature and ABS formation temperature. The gas outlet temperature directly correlates with the level of SO_2 to SO_3 conversion. Similarly, Figure 30 shows a direct correlation between SCR inlet NO_x and ABS formation temperature. The inlet NO_x directly correlates with NH_3 injection. SO_3 and NH_3 would directly related to ABS formation, with increased level of both SO_3 and NH_3 leading to early formation of ABS in the flue gas at high flue gas temperatures. It should be noticed the inflection in the curves in Figure 30 indicating still a lack of fidelity

of Model 5 on providing monotonic trending for the prediction of ABS formation
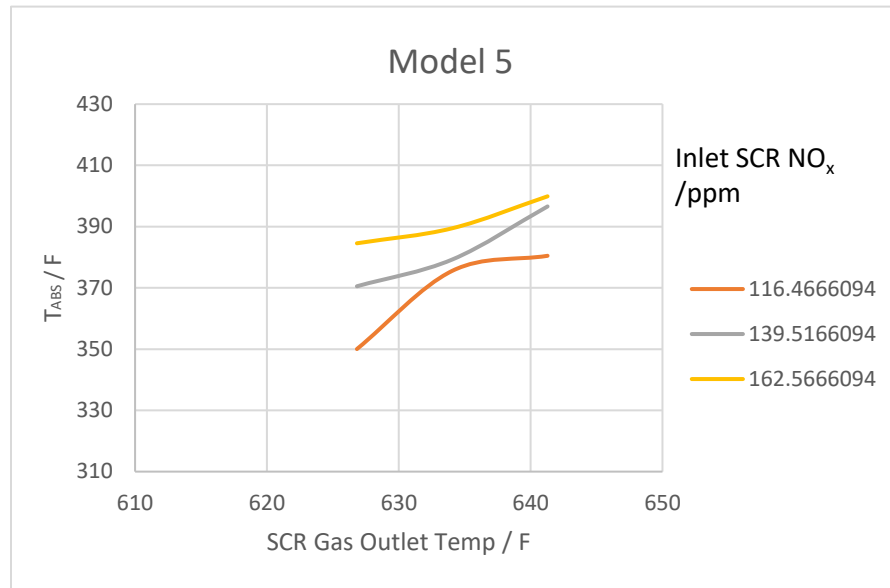
temperature.

Figure 30. Two Inputs Sensitivity Analysis for Model 5

Additionally, Figures 31 and 32 show contour plots of sensitivity analysis result between

variables and the ABS formation temperature for Model 5. Figure 31 shows the relationship

between ABS formation temperature, and SCR inlet NO_x and SCR gas outlet temperature.

From Figure 31, it can be seen that ABS formation temperature has positive correlation

with SCR inlet NO_x and SCR gas outlet temperature. The model shows some deficiencies

as the gas outlet temperature approach the larger part of the temperature range. Figure 32

shows the relationship between ABS formation temperature, and dilution ammonia flow

and SO_2 concentration. ABS formation temperature increases as the ammonia flow

increases, except for the low ammonia flow region. The increase of SO_2 concentration also

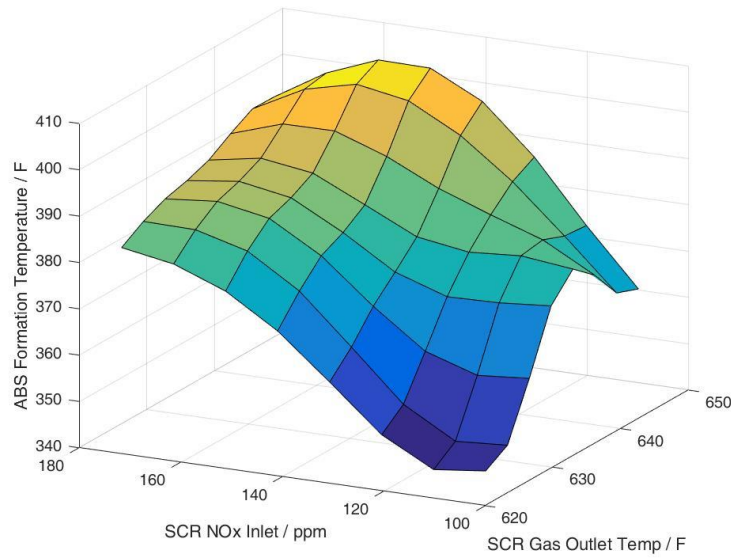leads to the rise of ABS formation temperature.

Figure 31. Relationship between ABS Formation Temperature, and SCR Inlet NO_x and
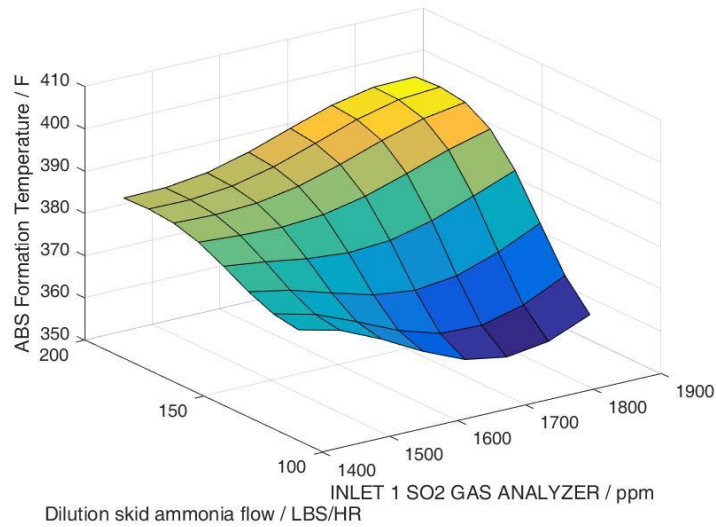SCR Gas Outlet Temperature

Figure 32. Relationship between ABS Formation Temperature, and Dilution Skid
Ammonia Flow and SO_2 Concentration

5. CONCLUSIONS AND RECOMMENDATIONS

Monitoring ABS formation temperature is very important in ABS fouling control in coal-fired power plants. If ABS formation temperature is known, boiler operators could take appropriate approaches to mitigate ABS fouling of air preheaters. However, it is difficult and expensive to accurately measure ABS formation temperature on-site. Researchers have performed modeling based on the thermodynamic equilibrium and performed bench scale experiments to find relationships between ABS formation temperature and the product of SO_3 and NH_3 concentrations. Data on the concentration of SO_3 and NH_3 are not readily available in power plants as well. Thus, the concept of indirectly inferring ABS formation temperature from readily available measurable parameters in power plants was studied. Based on data from Cayuga power station, five models were developed from data mining algorithms for the prediction of ABS formation temperature. Principal Component Analysis and Sensitivity Analysis were used to reduce the number of variables in the data set. K-Means Clustering was employed to compress the data samples. Neural Networks and Support Vector Machine were the two methods used to model data. The best model constructed in this study was built on four variables: SO_2 concentration, SCR gas outlet temperature, ammonia flow, and SCR inlet NO_x. These four variables were chosen since concentration of SO_3 and NH_3 are the key factors affecting ABS formation temperature. SO_2 concentration and SCR gas outlet temperature are related to SO_3 conversion. Ammonia flow and SCR inlet NO_x are related to NH_3 slip. This model was tested using all training

and testing samples. The NRMSE of the Model achieved 8.8%.

Data mining provides an interesting approach to indirectly infer ABS formation temperature. However, the models developed in this study still contain limitations. They can not provide good prediction when ABS formation temperature is below 340°F. Additionally, the best available model does a good prediction on ABS formation temperature only in full-load condition. Therefore, a more general model needs to be exhibited in future work. New data mining modeling should be explored using data from more than one plant and covering a broad range of operating conditions and variable readings. The fidelity of the new model should be assessed with bench scale experiments to prove the merit of the artificial intelligence approach.

REFERENCES

[1] https://www.worldcoal.org/coal/uses-coal/coal-electricity

[2] *Assessment of Air Preheater Fouling due to Utilization of SNCR and SCR Systems*, Wayne Counterman, Rui Afonso, Stratos Tavoulareas, EPRI GC-111797, December 1998

[3] *Steam*, edition 41, The Babcock & Wilcox Company

[4] https://en.wikipedia.org/wiki/Selective_catalytic_reduction

[5] *SELECTIVE CATALYTIC REDUCTION (SCR) OF NO BY AMMONIA OVER V2O5/TiO2 CATALYST IN A CATALYTIC FILTER MEDIUM AND HONEYCOMB REACTOR: A KINETIC MODELING STUDY,* M. Nahavandi, Brazilian Journal of Chemical Engineering, Department of Chemical and Materials Engineering, University of Idaho

[6] *Ammonia Bisulfate Formation Temperature in a Bench-Scale Single-Channel air preheater*, J.menasha, D. Dunn-Rankin, L.Muzio, and J.Stallings, Fuel, Department of Mechanical and Aerospace Engineering, University of California Irvine, Fossil Energy Research Corporation, Laguna Hills

[7] *Heat exchange surface for air preheaters*, Hilmer Karlsson Per, John Vickland, US 2432198 A

[8] *The Ljungström Air Preheater 1920*, An International Historic Mechanical Engineering Landmark, June 21, 1995, Stockholm, Sweden

[9] *Ammonia Sulfate and Bisulfate Formation in Air Preheaters*, J.M.Burke and

K.L.Johnson, Industrial Environmental Research Laboratory, Research Triangle Park NC 27711

[10]http://sdhengtao.en.made-in-china.com/product/eKaQbmFCEZkf/China-ASME-Standard-Rotary-Type-Air-Preheater-Enameled-Heating-Elements.html

[11] *Deposition of Ammonium Bisulfate in the Selective Catalytic Reduction of Nitrogen Oxides with Ammonia*, Shimpei Matsuda, Tomoichi Kamo, Akira Kato, and Fumito Nakajima, Hitachi Research Laboratory, Hitachi Ltd, Hitachi-shi, Ibaraki-ken, 319-12 Japan

[12] *Inferential sensor for on-line monitoring of ammonium bisulfate formation temperature I coal-fired power plants*, Fengqi Si, Carlos E.Romero, Zheng Yao, Fuel Processing Technology 90(2009)56-66

[13] *OPTIMIZING COMBINED BOILER-SCR OPERATIONS*, Lehigh Energy Update, Jan. 2009, Vol 27, No 1

[14] https://en.wikipedia.org/wiki/Principal_component_analysis

[15] *Principle Component Analysis*, Jolliffe, Series: Springer Series in Statistics, 2nd ed., Springer, NY, 2002, XXIX,487 p. 28,321-337

[16] https://en.wikipedia.org/wiki/K-means_clustering

[17] Algorithm AS 136: *A K-Means Clustering Algorithm*, J. A. Hartigan and M. A. Wong, http://www.jstor.org/stable/2346830

[18] *Support Vector Regression*, Debasish Basak, Srimanta pal, Dipak Chandra Patranabis, Neural Information Processing – letters and Reviews, Vol.11, No.10, October 2007

[19] *Sensitivity Analysis for Importance Assessment*, Andrea Saltelli, Risk Analysis. (2002).22 (3): 1–12

[20] *Application of support vector machine (SVM) for prediction toxic activity of different data sets*, C.Y. Zhao, H.X. Zhang, X.Y. Zhang, M.C. Liu, B.T. Fanb, Toxicology 217 (2006) 105–119

[21] *Ammonium Bisulfate (ABS) Measurement for SCR NO_x Control and Air Heater Protection*, Chetan CHothani, Robert Morey, MEGA 2008

[22] Neuframe is a software developed by Neural Computer Sciences

Vita

Fengxiang Nie was born on December 24, 1992 in Zhuzhou, China, son of Jingming Nie and Ping He. After finishing high school in 2011, he entered Southeast University and studied in the field of Thermal Energy and Power Engineering. He completed his Bachelor of Science in Thermal Energy and Power Engineering in 2015. After completing the B.S., he entered Lehigh University in 2015. He is currently a graduate student at Lehigh University.